HHS Public Access

Author manuscript

ACS Nano. Author manuscript; available in PMC 2022 May 25.

Published in final edited form as:

ACS Nano. 2020 December 22; 14(12): 16472–16501. doi:10.1021/acsnano.0c08356.

Toward Informed Design of Nanomaterials: A Mechanistic Analysis of Structure–Property–Function Relationships for Faceted Nanoscale Metal Oxides

Holly E. Rudel,

Department of Chemical and Environmental Engineering and Nanosystems Engineering Research Center for Nanotechnology-Enabled Water Treatment (NEWT), Yale University, New Haven, Connecticut 06511, United States

Mary Kate M. Lane,

Department of Chemical and Environmental Engineering and Nanosystems Engineering Research Center for Nanotechnology-Enabled Water Treatment (NEWT), Yale University, New Haven, Connecticut 06511, United States

Christopher L. Muhich,

Nanosystems Engineering Research Center for Nanotechnology-Enabled Water Treatment (NEWT), Yale University, New Haven, Connecticut 06511, United States; School for the Engineering of Matter, Transport, and Energy, Ira A Fulton Schools of Engineering, Arizona State University, Tempe, Arizona 85001, United States

Julie B. Zimmerman

Corresponding Author: julie.zimmerman@yale.edu. Complete contact information is available at: https://pubs.acs.org/10.1021/acsnano.0c08356.

Supporting Information

The Supporting Information is available free of charge at https://pubs.acs.org/doi/10.1021/acsnano.0c08356.

Crystallographic data used for CeO_2 in Figure 2 (CIF)

Crystallographic data used for Co_3O_4 in Figure 2 (CIF)

Crystallographic data used for Cu_2O in Figure 2 (CIF)

Crystallographic data used for hematite α-Fe_2O_3 in Figure 2 (CIF)

Crystallographic data used for cassiterite SnO_2 in Figure 2 (CIF)

Crystallographic data used for anatase TiO_2 in Figure 2 (CIF)

Crystallographic data used for zincite ZnO in Figure 2 (CIF)

The authors declare no competing financial interest.

VOCABULARY

exposed crystal facet	descriptor of the surface plane of atoms in a crystalline material
Miller indices	denotation of the crystal plane of a nanoscale metal oxide, derived from the orientation of the lattice plane and defined as the reciprocals of the intersection of the plane on the *x*, *y*, and *z* axes
Fermi level	topmost filled electron energy state at absolute zero
Sabatier Principle	qualitative concept in heterogeneous catalysis that states that the interaction between reactants and catalyst surface should be of intermediate strength to promote high catalytic activity
Tasker type surface	description of the distribution of charges on the crystal planes of nanoscale metal oxides; type 1 is nonpolar with equal anions and cations on each plane; type 2 has alternating charged planes but no net dipole moment; type 3 has charged planes and a dipole moment normal to the surface

Department of Chemical and Environmental Engineering, Nanosystems Engineering Research Center for Nanotechnology-Enabled Water Treatment (NEWT), and School of Forestry and Environmental Studies, Yale University, New Haven, Connecticut 06511, United States

Abstract

Nanoscale metal oxides (NMOs) have found wide-scale applicability in a variety of environmental fields, particularly catalysis, gas sensing, and sorption. Facet engineering, or controlled exposure of a particular crystal plane, has been established as an advantageous approach to enabling enhanced functionality of NMOs. However, the underlying mechanisms that give rise to this improved performance are often not systematically examined, leading to an insufficient understanding of NMO facet reactivity. This critical review details the unique electronic and structural characteristics of commonly studied NMO facets and further correlates these characteristics to the principal mechanisms that govern performance in various catalytic, gas sensing, and contaminant removal applications. General trends of facet-dependent behavior are established for each of the NMO compositions, and selected case studies for extensions of facet-dependent behavior, such as mixed metals, mixed-metal oxides, and mixed facets, are discussed. Key conclusions about facet reactivity, confounding variables that tend to obfuscate them, and opportunities to deepen structure–property–function understanding are detailed to encourage rational, informed design of NMOs for the intended application.

Graphical Abstract

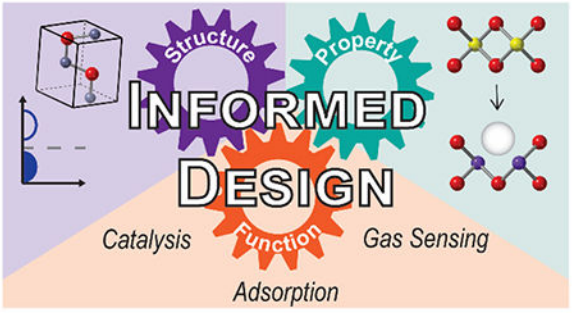

Keywords

nanoscale metal oxides; facet engineering; catalysis; gas sensing; sorption; crystal facet; informed design; structure–property–function relationships

Nanoscale metal oxides (NMOs) have received increasing attention in a variety of environmental fields including catalysis, gas sensing, and contaminant sorption.[1–4] At the nanoscale and with decreasing size, these materials have the dual benefit of a large effective surface area and increased reactivity. The high activity of NMOs facilitates adsorption of oxidizing species and/or target molecules to the surface. Specifically, earth-abundant NMOs are promising sustainable and cost-effective alternatives to scarce metal and metal oxide catalysts, gas sensors, and sorbents. However, in order to fully realize the power and potential of these NMO technologies and compete with highly reactive, but environmentally and economically expensive, rare-earth materials, optimizing the performance of NMOs in

their respective applications is essential. Because this performance is inextricably linked to the interactions at the surface, elucidating the drivers of interfacial reactivity is necessary to inform design of highly functional materials in their intended applications.

Conventional understanding is that the smaller the NMO size, the higher the surface area, resulting in additional surface-like interactions that promote chemical and physical properties that are remarkably different from bulk.[4,5] Consequently, much attention has focused on increasing the surface area of synthetic NMOs to increase functional performance.[6] However, recent studies[7,8] have demonstrated that smaller size does not necessarily correlate with an increase in reactivity, suggesting that other aspects in addition to surface area contribute to NMO reactivity. Indeed, significant research on the functionality of NMOs has been attributed not just to the quantity of exposed surface but also to the structure and composition of that surface for controlling reactivity.[8–12]

In fact the exposed crystal surface, or facet, has been shown to offer greater control than size on the nanoscale in tuning the reactivity of a metal oxide.[13] With different facets exposing different surface atoms, tuning NMO morphology correspondingly controls its surface chemistry and reactivity. This is important when considering the (intrinsically linked) structural and electronic factors that contribute to binding target molecules. Depending on the atomic coordination and structural configuration of NMO surfaces, different proportions of cations and anions are accessible for reactant adsorption, thus greatly influencing the charge transfer between sorbent and sorbate and affecting the type and strength of binding and generation of products or reactive species. Furthermore, different atomic coordinations result in distinct electron density configurations, also influencing the type and strength of binding as well as electron band gap energies and positions. Because these electronic and binding characteristics and behaviors govern the mechanisms of sorption-dependent fields such as heterogeneous catalysis, gas sensing, and contaminant removal, it is unsurprising that the exposed crystal plane contributes to NMO performance in these applications.

Through a combination of experimental and computational methods, it has become generally accepted that there is an inverse correlation between the stability (surface energy) and reactivity of a metal facet.[2,3] Beyond surface energies, a complex amalgamation of characteristics contribute to important surface processes that determine reactivity, in varying degrees of significance depending on the application: the presence of surface defects; surface sorption/desorption ability; redox potential; surface area; coordination of surface atoms; concentration, energy, and mobility of oxygen vacancies; and electronic band structure.[14] A robust understanding of these fundamental aspects of NMO facets will inform design of materials that are optimized for a given application.

In this review, we first describe the fundamental mechanisms that govern bonding behaviors, specifically sorption, a critical first step in many surface-mediated reactions, on metal oxide surfaces. We next depict the atomic and electronic structures of different crystal facets focusing on common NMOs: cerium oxide, cobalt oxide, cuprous oxide, iron oxide (hematite), tin oxide, titanium dioxide, and zinc oxide. We expound upon the underlying structural and electronic characteristics of these NMOs by discussing mechanisms in catalytic, gas sensing, and contaminant sorption applications and examining experimental

and computational studies of high- and low-reactivity facets. We highlight extensions of facet-dependent reactivity including mixed-metal-oxide nanomaterials, metal-metal-oxide support-structure materials, and mixed-facet materials, while relating the underlying performance back to inherent structural characteristics of individual NMO facets. Finally, areas within the field of facet engineering that require further development are detailed, including opportunities for exploiting surface characteristics to impart selectivity. This review increases understanding of *why* certain facets are observably better performing, rather than to simply detail *that* they are better performing. This foundation will enable the informed design of next-generation materials that will inspire solutions for our world's most pressing environmental problems.

MECHANISMS OF BONDING BEHAVIOR

The ability and strength of adsorbates to bind on metal oxides depend on the atomic and electronic structures of both species. These structures are inter-related, where the atomic positions dictate the electronic structure, and the electronic structure dictates the energy, and thus stability, of the atomic positions. At the simplest level, the atomic geometry controls the number and availability of reactive sites. Because most bonding on metal oxides occurs at the cationic site, the accessibility of the cation is critical. If all of the cations are entirely buried beneath O anions, they are inaccessible and adsorption is unlikely. Notably, the opposite is true for positively charged species, such as protons, which bond ionically to O anions. The local geometry controls the atomic coordination, and thus, the electronic state of the atoms, such as the number of dangling bonds and oxidation states. These steric and electronic effects control mechanisms by which bonding can happen and form the basis of the relationship between surface structure and bonding behavior and strength. The electronic structure largely dictates bonding behavior. Polar/ionic and covalent, including dative, bonding provides the structure for the following discussion because they are representative of many adsorbate/metal-oxide bonds.

The electronic structure is often represented through a density of states plot (Figure 1). The density of states for each different facet of a metal oxide is distinct, resulting in important binding implications that are discussed throughout the remainder of this review. In most metal oxides, the Fermi level sits at the edge of the valence band (VB), which is mostly composed of O 2p states, while the conduction band (CB) is usually empty and composed of metal d or f states. An empty CB and completely filled VB (Figure 1a) indicate that the O are oxidized and the metals are positively charged. For the same material, different facets may have higher or lower energies, which correspond to shifts in the band edge energies and the associated Fermi level (Figure 1b). Raised Fermi levels/band edges increase the energy of electrons, making them more reactive. Further, if O vacancies (V_os) are present, electrons are transferred to the CB providing high-energy localized electrons (Figure 1c,d). These excess electrons can facilitate strong chemical bonds between reactants and NMO surface. Additionally, the delocalized electrons adjacent to the oxygen vacancy (V_o) are more likely to be excited, enhancing the NMO's catalytic performance.[15] The importance of V_os, both their generation and exchange, are well-documented in catalytic applications because of the enhanced reactivity of these high-energy electrons.[16–20] If cationic vacancies are present, holes form at the O 2p VB edge, providing high-energy holes that attract electrons.

Polar and ionic bonds form from the Coulombic attraction of charged species, such as electron lone pairs and positively charged cations, without the direct sharing of electrons. The presence of multiple charged species in an adsorbate increases the adsorption strength to metal oxides by providing multiple Coulombic attractions. For example, both the protons and oxygen atoms of water can form bonds to the surface O anion and metal cation, respectively. The strength of the bond depends on the degree of oxidation of the cation (controlled by the electronic structure), the accessibility of the cationic site (controlled by the geometric structure), and the polarity or oxidation state of the adsorbate.

Nonpolar and less polar species require the formation of covalent bonds to chemisorb. The required sharing or exchange of electrons necessitates several electronic structural features. Because the oxygen ions tend to be fully oxidized (having full octets), the ability of sorbates to form covalent type bonds generally requires electronic interactions between the surface sorbent and metal cations. If filled orbitals of the potential adsorbate overlap in energy with filled or available metal states, the orbitals can rearrange themselves to form bonds between surface and adsorbate. More commonly, dative bonds are required, for example the adsorption of O_2. Here, only one of the species donates electron density to form the covalent bond, (*i.e.*, the surface or the adsorbate). This requires that the electron density from the donating species is higher in energy than the newly forming orbital. For example, high-energy electron density in the CB of the metal-oxide sorbent can be transferred to the incoming adsorbate to form the bond, as is required for O_2 adsorption (Figure 1d), but without the high energy density, no bond forms (Figure 1c).[21,22] The formation and strength of covalent, and particularly dative bonds, are highly dependent on the energy of the band edges relative to the orbitals of the adsorbate, as slight variations can preclude electron donation or misalignment of forming bonds. Because surface termination modulates the energy of the bands and the number of vacancies, this has direct control over the adsorbate strength and capacity.

Clearly, the structure and configuration of exposed surface atoms is intrinsically linked with the ability of the surface to bind with adsorbates. Because this binding derives from the compatibility of electron densities and energies between sorbent and sorbate, each NMO uniquely exhibits facet-dependent behavior. For example, despite α-Fe_2O_3 and α-Al_2O_3 having nearly identical atomic structures, differences in their electronic makeup result in differences in reactivity.[23] It is therefore critical to understand both the surface atomic and electronic structures of NMOs, how it may change under different reaction conditions, and how these characteristics contribute to enhanced reactivity in various applications.

ATOMIC AND ELECTRONIC CHARACTERISTICS OF NMO FACETS

The understanding of metal oxide surface structure and interfacial interactions has rapidly increased over the past few years. Advances in computational modeling and analytical techniques have enabled precise probing of metal oxide surfaces. This section surveys the current state of knowledge on the atomic and electronic structures of low-index facets of the NMOs: cerium oxide, cobalt oxide, cuprous oxide, iron oxide (hematite), tin oxide, titanium dioxide, and zinc oxide (Figure 2a–g). For crystal structures, low-index crystal facets are those where all three Miller indices (*hkl*) are either zero or ±1(Figure 2h). These

facets often possess the lowest surface energy and are the most thermodynamically stable. For corundum-structured oxides (*i.e.*, hematite), the "R-cut" {012} surface is a natural growth face, which also has low surface energy and high thermodynamic stability.[24,25] Consequently, in typical syntheses, these low-index facets do not require excessively high temperatures or harsh surface-directing agents. They are also less likely to reconstruct during or after the synthesis process when compared with unstable (but also described as "better performing") high-index facets and have thus been strategically selected to be the focus of this review. Despite being relatively low-energy, low-index facets can have surface instabilities due to their crystal plane structuring. Polar planes, often categorized by their Tasker classifications, are particularly susceptible to this reconstruction and reordering to reduce surface energy.[26,27] This reconstruction is important because it can result in surface defects such as steps, kinks, or vacancies, known to be active sites.

Two important notes on this discussion include the conditions in which experiments were conducted and whether nanoparticles were directly studied. Excellent studies of surface structure have been done in ultrahigh vacuum (UHV), where almost no amount of water vapor is present, that have elucidated fundamental knowledge of surface structure. However, for designing NMOs for environmental applications, characterizations under environmentally relevant conditions are more pertinent. Relatedly, selection of the surface structure and *in situ* conditions in computational models, especially when used to explain or corroborate experimental observation, must be critically evaluated as these choices can influence the thermodynamic stability of metal oxide surfaces. A mismatch between experimental and computational surface structures will obfuscate true surface structure reactivity conclusions.[28] Next, many surface studies utilized single crystal metal oxides cut to expose a particular surface, rather than on nanoparticles. As many of the properties of particles change on a nanoconfined scale, it is imperative that continued study of the structure and relaxation of NMO facets continues to develop with the advancement of characterization techniques (see Future Directions and Opportunities).

Cerium Oxide.

Cerium oxide, or ceria (CeO_2), has a cubic fluorite ($Fm\bar{3}m$) structure with a face-centered cubic array of metal atoms with oxygens positioned at tetrahedral sites (Figure 2a).[29] CeO_2 is a wide-band-gap semiconductor with a VB of predominantly oxygen 2p character, a CB with primarily cerium 5d character, and localized, empty 4p electron states in the band gap.[30] It has been one of the most well-studied metal oxides because of its catalytic performance in a variety of applications including contaminant degradation, automotive three-way catalysts, and CO oxidation as well as organic synthesis and hydrogenation reactions.[11,31,32] Even under reducing conditions that induce the loss of a considerable amount of oxygen from its lattice (and subsequently a high density of V_os), ceria retains its structure and can be reoxidized by exposure to an oxidizing environment, meaning that it can accommodate rapidly formed and eliminated vacancy defects, critical to effective catalytic applications (see Catalysis).[29] For these reasons, ceria is classified as having a high oxygen storage capacity.[33,34] When V_os are created under high temperatures and/or reducing conditions (such as during catalytic reactions), these vacancies are charge-balanced by the formation of Ce^{3+} defects.[30,35] Critically, the ceria's reduction entropy (generation

of V_os) is quite large due to the single-electron population of the 4f orbitals.[30,36] The reduction entropy enables reactions that, from an enthalpic perspective, would be endergonic or require very high temperatures, such as thermochemical fuel production.[36–38]

The {100}, {110}, and {111} facets are the three most thermodynamically stable surfaces of ceria.[35] The nonpolar {111} facet of ceria is generally reported to be the most stable surface and the least reactive due to a lower proportion of oxygen and cerium vacancies compared with the {100} and {110} surfaces.[11,39] It is terminated by oxygen layers that are singly undercoordinated, though, due to the relative size of the O atoms and atomic structure, the Ce cations are also accessible.[11,35] The {111} facet is the most compact, and thus less likely to accommodate a vacancy defect (as reflected in its high vacancy formation energy).[11,40] It is classified as a Tasker type II surface, where each plane is charged, but due to symmetry, there is no net dipole moment.[11,35]

The {110} surface exposes both O and Ce, and the surface layer is nonpolar due to a stoichiometric balance between the two atoms, classified as a Tasker type I surface.[11,35] The surface O and Ce ions are undercoordinated by 1 and 2 bonds, respectively. Calculations on this surface indicate that the Ce contracts into the bulk slightly more than O.[41] DFT calculations show that the {110} surface has the lowest energy of V_o formation, which affects performance in catalytic applications.[42]

The {100} face of CeO_2 is the least stable, and most reactive, low-energy surface of ceria. It is a Tasker type III surface with alternately charged planes that produce a net dipole moment.[11] {100}-faceted nanocubes have been shown to possess a larger band gap compared with the {110}–{100}-faceted nanorods.[43] Because of this instability from surface polarity, the {100} surface may undergo significant surface reconstruction, whereby half of the surface oxygen anions are released to the gas phase.[40,44,45] The structural characterization of the {100} surface is still debated, especially the configuration of the oxygen anions, which depends on synthesis conditions and postsynthesis treatments. Therefore, it is unlikely that it is terminated by a single layer of either Ce or O, but rather by a combination. The exposed O and Ce ions are at least 2-fold undercoordinated. Both the {100} and {110} surfaces have 6-fold-coordinated Ce at the surface, with two dangling bonds, compared with the 7-fold-coordinated Ce on the {111} surface.[11,35]

The different facets of CeO_2 also have different acid–base properties, where O serves as basic sites and Ce as acidic sites. Wu *et al.* found using IR spectra that the Ce atoms are only weak Lewis acid sites and that the acidity is largely independent of nanoparticle morphology, while, conversely, oxygens are much more basic and their basicity follows a clear trend of octahedra (majority {111} exposed facets) < cubes (majority {100}) < rods (majority {110}).[46] A recent study by Chen *et al.* utilizing a more powerful NH_3 temperature-programmed desorption method found small trends in acidity with morphology: for weak and medium acid sites, nano rods (majority {111}) < cubes (majority {100}) < rods (majority {110}), along with cubes (majority {100}) having the most strong acid sites.[32] The weak morphology dependence of acid sites arises from a compensation between the number of site types and the site type acidity. Therefore, despite Ce^{4+} being more basic than Ce^{3+}, Ce^{4+} atoms are less exposed than Ce^{3+} atoms, which counterbalances

their increased basicity. Although {110}-rods and {100}-cubes have a higher coordinative unsaturated status compared with the {111}-octahedra, the portion of weaker Lewis sites is larger, resulting in similar acidity across morphologies.[46] The surface basicity is strongly correlated with the morphology-dependent defect density and inversely correlated with V_o formation energy.[41] These differences in acid–base properties have been shown to largely direct catalytic behavior, with a higher density in acid–base sites correlating with enhanced catalytic behavior.[47,48]

Cobalt Oxide.

Cobalt(II,III) oxide (Co_3O_4) has a spinel structure ($Fd\bar{3}m$), with Co^{3+} in an octahedral coordination and Co^{2+} in a tetrahedral coordination and the oxygen atoms forming a distorted face-centered cubic sublattice (Figure 2b).[49] This mixed valence structure improves the bifunctional behavior of Co_3O_4 for applications such as oxygen evolution reactions (OER) and oxygen reduction reactions (ORR) by providing donor–acceptor sorption sites for oxygen species.[50] Co_3O_4 has also been well-studied for catalytic activities in low-temperature CO oxidation, again because of the coexistence of Co^{2+} and Co^{3+}.[51] The most common crystal planes of Co_3O_4 are the {100}, {110}, and {111} planes, with {110} and {111} naturally occurring.[52] The {110} plane can have two types of surface terminations: type A, which contains a mixture of tetrahedral Co^{2+} cations, octahedral Co^{3+} cations, and O^{2-} anions and is cationic in nature; type B, which contains Co^{3+} cations and 2-fold- and 3-fold-coordinated O^{2-} anions and is anionic in nature, though both primarily expose O atoms.[52–54] Type A and type B have different stability and reactivity, and transition between the two is achieved by controlling the synthetic conditions, including oxygen partial pressures.[52,54] The {111} surface can be terminated by Co^{2+}, Co^{3+}, O^{2-}, or a mix of the three depending on the oxidative environment, though typically the Co^{2+} and O^{2-} termination is most often used as the active site structure.[53,55] Compared with the {110} and {111} surfaces, the {100} facet has a lower density of both Co^{2+} and Co^{3+} and is generally more stable.[56] The calculated surface energies of low-index Co_3O_4 crystal planes follows {100} < {111} < {110}.[57] However, the presence of water leads to surface hydroxylation, and at various temperatures, this ordering has been shown to flip to {111} < {100} < {110}.[57]

Cuprous Oxide.

Cuprous oxide (Cu_2O) has a cubic crystal structure ($Pn\bar{3}m$), where an oxygen body-centered cubic lattice is surrounded by tetrahedra Cu(I) atoms forming a face-centered cubic lattice (Figure 2c).[2] It is a direct band gap semiconductor and has been studied as both a gas sensor and a catalyst.[3,58] The common, low-index exposed facets are {100}, {110}, and {111}.[2,59] The {110} facet contains both Cu and O atoms at the surface, with the copper atoms fully exposed. This surface contains both doubly coordinated Cu (Cu_{2c}) atoms and undercoordinated, singly coordinated Cu (Cu_{1c}), making it positively charged with a dangling bond perpendicular to the surface.[2,58] The {111} facet similarly exposes both Cu atoms and O atoms, but the density of dangling bonds is much less than the {110} surface.[58,59] This surface is classified as a Tasker type II surface and contains only some fully exposed Cu atoms, with the others blocked by surface oxygen atoms.[2,60] Multiple surface structures of the {100} surface (including a copper-terminated and oxygen-

terminated structure) have been observed depending on surface annealing and oxygen partial pressures.[61] Unreconstructed, the copper-terminated {100} is expected under oxygen lean conditions and is polar with alternating Cu^{+} and O^{2-} layers and a net dipole moment perpendicular to the surface (Tasker type III).[61] However, this surface is expected to undergo significant reconstruction to reduce surface polarization. The oxygen-terminated {100} is expected under elevated oxygen pressures.[61] Regardless of the termination, the surface Cu atoms have been shown to be coordinatively saturated, resulting in an electronically stable state, and only partially exposed.[2,58] The surface energies of Cu_2O generally follow the density of undercoordinated Cu atoms, {100} < {111} < {110}. The surface energy generally correlates with catalytic performance of Cu_2O nanocrystals, as measured by cubic {100} crystals, octahedral {111} crystals, and rhombic dodecahedral {110} crystals.[58,59]

Iron Oxide (Hematite).

Hematite (α-Fe_2O_3) has a hexagonal unit cell and a corundum-type structure ($R\bar{3}c$), with two-thirds of the sites filled with regularly arranged Fe^{3+} ions (Figure 2d).[62] While naturally abundant in rocks and soils, synthetic hematite has shown wide applicability in the fields of catalysis and environmental remediation as a low-cost, environmentally friendly alternative to rare-earth metals.[1,62]

The most commonly studied facets of hematite are {001}, {110}, and {012}, though different atomic terminations are known to exist under different preparation methods and environmental conditions.[63] Despite many surface structure studies being conducted in vacuum conditions, the structure and stability of different hematite facets changes in the presence of water, which clearly is the case in photocatalytic degradation of aqueous pollutants or sorption of aqueous contaminants, two of the most well-studied applications of hematite NMOs.[64–66] The {110} surface is perhaps the most straightforward, as it is generally accepted that the {110} surface has one surface termination: a ridge-and-valley topography, with singly and doubly coordinated groups in the ridges and doubly and triply coordinated groups in the valleys.[66,67]

In ultrahigh-vacuum conditions, the {012} surface is terminated with Fe in 5-fold coordination (Fe_{5c}) and oxygen anions in 3-fold coordination (O_{3c}) in a zigzag pattern.[68] At higher temperatures, however, a partially reduced reconstructed surface is possible. In aqueous conditions, water reacts on this surface, resulting in a structure with terminal and bridging (hydr)oxo groups. The {012} surface has two stable ridge-and-valley terminations that can coexist in aqueous solution: the full-layer termination and the half-layer termination.[69] In the half-layer termination, the topmost Fe layer of the repeating Fe_2O_3 sequence is vacant, and the surface has singly, doubly, and triply coordinated (hydr)oxo groups.[68,70] The full-layer termination has an additional O layer, resulting in a charge-neutral stochiometric surface. The full-layer ridge-and-valley topography has singly coordinated hydroxyl groups on the ridges and triply coordinated hydroxyl groups in the valleys (no doubly coordinated hydroxyl groups).[69,71] The full-layer termination is dominated by singly undercoordinated iron sites, but the half-layer termination has a reduced density of these sites.[72] While both terminations contain singly and triply coordinated terminal oxygens, the half-layer termination also contains doubly coordinated

oxygens, known to be less exchangeable.[73,74] Comparison of the reflectivity profiles suggests that the half-layer termination is the dominant termination in water but that some full-layer termination exists.[69,73,75,76]

The clean {001} facet has been reported to have three different terminations: a single Fe termination, a double Fe termination, and an O termination.[77] The Fe single termination and O termination have been observed as coexisting and are variably stable depending on the oxygen partial pressure, oxidation conditions, annealing temperature, and whether the measurements are done in a dry or humid/aqueous environ-ment.[65,77–79] It has been suggested that the single Fe termination is the most stable in the oxygen-poor range, but in oxygen-rich atmosphere, the surface becomes oxygen-terminated.[77,80] More recent work indicates that the Fe-layer termination is the most stable and is dominated by 3-fold undercoordinated iron.[72,81]

Given that the termination structure of hematite is widely debated, there are resulting inconsistencies across studies. This difference in surface termination is important due to the varying amounts of singly, doubly, and triply coordinated (hydr)oxo groups and different iron (under)coordinations, which are especially important in ascertaining surface reactivity.[79] Surface energies also vary across studies with Mackrodt calculating {012} < {001} < {110},[82] and Guo and Barnard finding the OH-terminated surface energy to follow O-terminated {001} < {012} < Fe-terminated {001} < {110}, because the hydroxylation of the O termination reduced the surface energy significantly.[83]

Tin Oxide.

Tin(IV) oxide (SnO_2) exists in a tetragonal rutile-type structure ($P4_2/mnm$) in its most stable form. Each tin atom is coordinated by six oxygen atoms positioned at the vertices of a distorted octahedron where four more oxygen atoms lie in the same plane (Figure 2e).[3] Low-energy facets of SnO_2 are {110}, {101} (same as {011}), and {100} (same as {010}), with the surface energies following {110} < {100} < {101}.[84] However, under reducing conditions, the ordering has been found to change to {101} < {110} < {100} and the structures likely reconstruct.[84] The nonpolar {110} surface contains rows of 5-fold-coordinated Sn atoms (Sn_{5c}) and one dangling bond perpendicular to the surface.[85,86] This surface exhibits a multitude of surface reconstructions depending on preparation conditions, influencing both the atomic and electronic structures.[87] The {101} surface possesses all Sn atoms with Sn_{5c} and one dangling bond perpendicular to the surface.[85]

Titanium Dioxide.

Titanium dioxide, or titania (TiO_2), rutile ($P4_2mnm$) and especially anatase ($I4_1amd$) polymorphs are the most well-studied NMOs in photocatalysis because of their long-term stability, benign nature, strong oxidizing power, high photochemical activity, and inertness to chemical attack.[8,14] Both crystals are tetragonal in structure and formed by chains of distorted TiO_6 octahedra.[88] Anatase is less dense than rutile, and though the coordination is the same, the octahedra are significantly more distorted. It is typically the more reactive form of TiO_2, because high charge carrier mobility enables transfer to the surface from much deeper in the bulk lattice.[89] Anatase is the more well-studied polymorph for catalytic

applications and thus will be the focus of this review (Figure 2f). The three low-index facets in anatase crystals are {001}, {010}/{100}, and {101}, with the {001} and {101} surfaces being the most well-studied. The {100} surface consists of 5-fold-coordinated Ti cations (Ti_{5c}) and 2-fold-coordinated O anions (O_{2c}).[90] The {101} surface has both 5-fold- and 6-fold-coordinated Ti atoms (Ti_{5c}, Ti_{6c}) and 2-fold- and 3-fold-coordinated O atoms (O_{2c}, O_{3c}).[88,90] On the {001} surface, only Ti_{5c} are present, as well as O_{2c} and O_{3c}. The reconstruction of the high-energy {001} facet under different environmental conditions is well-studied, with theoretical results supporting the conclusion that reconstruction of these facets impairs much of the facet reactivity.[13,90]

Because TiO_2 finds its major applications in photocatalytic processes, a brief discussion of electronic structures is warranted, though also described in excellent reviews.[8,13] Facet-dependent trends in electronic structure can often be muddied by confounding variables such as the presence of adsorbates or coexistence of multiple facets. However, reports generally support that {101} dominant anatase crystals have a slightly larger band gap compared with {001} (3.3 *vs.* 3.2 eV).[91,92] This is important because one of the drawbacks to TiO_2 structures for photocatalysis is the fact that the wide band gap necessitates the usage of UV light in order to excite electrons into the CB. Some DFT calculations also suggest that the {001} and the {101} facets possess the same VB, but the {101} facets have a higher CB edge.[93] Because of this, the electrons migrate toward the {101} facets and the holes migrate toward the {001} facets, allowing for heterojunction charge separation that has been shown to be favorable in photocatalytic applications (see Extensions of Facet Reactivity).[8,93]

Zinc Oxide.

Wurtzite-type ZnO ($P6_3mc$) has a hexagonal structure, with tetrahedral-coordinated zinc and oxygen atoms that are alternately stacked (Figure 2g).[3] The tetrahedral coordination results in a noncentral symmetric structure.[94] The low-index surfaces are the nonpolar {100} and {110} facets and the polar Zn-terminated (001) and O-terminated $(00\bar{1})$ facets.[95] The {001} surfaces are Tasker type III surfaces because of the dipole moment and spontaneous polarization along the *c*-axis.[94] However, these surfaces are atomically flat and stable and do not exhibit any surface reconstructions, making them abnormally stable for polar oxides,[94] though this is somewhat controversial, as recent research suggests that these surfaces actually do undergo reconstruction.[96] The {100} surface is mixed-terminated and classified as Tasker type I. It is the most energetically favorable and possesses a low density of defects (particularly V_os).[97] Though the {110} surface is less studied, it similarly is mixed-terminated and low energy (though slightly higher than the {100} surface).[97] Gao and Zhang calculated the density of dangling bonds on some of the stable ZnO crystal planes to follow {101} < {100} < {001}.[3] On the basis of these considerations, it is likely that the activity (based on surface energies and density of dangling bonds) of the ZnO facets would generally follow {100} < {110} < {001}, an ordering that is typically borne out in experimental studies (see Gas Sensing).

APPLICATIONS

For catalysis, gas sensing, and contaminant removal, different defining properties of NMOs are key to enhanced function. While certain NMOs demonstrate clear trends in facet-dependent performance, some studies conflict with one another, attributable to a variety of reasons:

1. NMO facets, especially polar facets and high-index facets, can reconstruct and/or aggregate under different preparation, reaction, and post-treatment conditions, resulting in different terminations and exposed surface atoms.[63,87]
2. Variable synthesis procedures can result in different densities of surface defects, an increase of which has been shown to improve charge separation and photon-to-electron conversions.[43,98]
3. The coexistence of multiple facets on synthesized nanoshapes can make it difficult to definitively ascribe singular facet behavior if relying on empirical studies alone.[11,99]
4. Identifications of exposed facet using high-resolution transmission electron microscopy, selected area electron diffraction, and/or X-ray diffraction studies are complex and precise endeavors, rendering the misidentification of exposed facets easily possible.[100,101]

The following sections will therefore primarily discuss the atomic and electronic characteristics conducive to enhanced performance in each application, with a supplementary analysis of which facet(s) demonstrate these conditions.

Catalysis.

NMOs have demonstrated success in a variety of catalytic applications including (photo)oxidation and non-oxidative reactions (Table 1). Due to the wide variability in catalytic reactions, no single descriptor determines which facets are most effective. Accordingly, NMO facet performance is evaluated in each catalytic application. As the most well-studied NMO in catalysis research, the structure–property–function relationships of TiO_2 are also the most well-developed, with numerous experimental and computational results highlighting the facet-dependent activity of its {001} and {101} facets.[102] Because these facet-dependent catalytic mechanisms and performances have been thoroughly detailed in a number of excellent reviews,[8,13,14,92,93] these results are summarized here while primarily focusing on the opportunities afforded by less well-studied catalysts with the hope that similar structure– property–function studies be conducted on these metal oxides to improve their application in these fields.

Catalytic Oxidation.—Unlike metallic catalysts, NMOs have the advantage of oxygen atoms (and corresponding V_os) in the lattice structure that can participate in the catalytic/redox cycle.[4] As a result, the ease of the oxidation reaction depends primarily on the energy that it takes to release the oxygen from the surface as well as the mobility of bulk oxygen to the surface.[4] Because each facet has a different surface atomic and band structure, the redox

characteristics (*e.g.*, oxygen storage capacities, V_o formation energies) are also varied and, thus, different facets show different efficiencies in catalyzing oxidation reactions.

Fenton and Fenton-like Catalysis.—Fenton and Fenton-like reactions, where hydroxyl radicals ($HO^•$) or reactive oxygen species (ROS) facilitate decomposition of organic pollutants, are some of the most common advanced oxidation processes because of ease of design and low toxicity of reagents used (Figure 3).[148,149] A range of Fenton and Fenton-like processes using NMO semiconductor catalysts have been studied for the degradation of organic contaminants,[148,149] most commonly, organic dyes including rhodamine B (RhB),[72] methylene blue (MB),[117] acid orange 7 (AO7),[150] and methyl orange (MO)[99] (Table 1, Figure 3). Generally, the external addition of H_2O_2 up to a certain concentration is known to expedite the ROS generation (beyond which H_2O_2 acts as a scavenger of $HO^•$ to produce the less powerful oxidant, perhydroxyl radical).[151–153] However, for conventional wastewater treatment, the high quantities of H_2O_2 needed to produce sufficient $HO^•$ for regulatory compliance is often prohibitive.[154] For this reason, some NMOs, particularly TiO_2, have been closely studied for their ability to (photo)generate H_2O_2 from O_2.[155]

Effective H_2O_2 activation requires the NMO metal to be stable in multiple oxidation states (to facilitate electron transfer to and from the oxidizing species) and is aided by the presence of V_os. Oxygen vacancies, which possess an abundance of localized electrons, are thought to be the active site for H_2O_2 activation because the back-donation of these localized electrons to sorbed H_2O_2 molecules facilitates their dissociation and break down to ROS.[156] The electronic structure of the exposed crystal facet is therefore crucial for the sorption and activation of H_2O_2, with higher densities of surface undercoordinated metals or V_os typically resulting in more reactive and more effective degradation of organic contaminants. These facets must also show a strong sorption affinity and capacity both for the contaminant of interest, which often depends on the charge and nature of the contaminant, the distribution of electrons near the NMO Fermi level, and the oxidizing agent (*i.e.*, H_2O_2). Recently, Zhang *et al.* demonstrated that a high density of V_os enhanced RhB degradation because these vacancies (1) bound RhB and H_2O_2 adsorbates more strongly due to an increase in charge density, and (2) stretched and weakened the O–O bond of adsorbed H_2O_2, resulting in enhanced H_2O_2 decomposition to active $HO^•$ radicals.[20] While some studies have suggested that surface hydroxyls can stabilize thermodynamically unstable V_o clusters and thus increase performance,[157] others have attributed lowered performance to the electrostatic repulsion between these groups and negatively charged organic dyes.[31]

TiO_2, a wide-band-gap semiconductor, has received extensive attention as a photocatalyst.[8,14,92,93] In 2009, Yang *et al.* synthesized {00l}-faceted anatase TiO_2 nanosheets that were exceptional in photogenerating $HO^•$ radicals in an aqueous solution due to a high density of undercoordinated Ti atoms.[158] Since then, research interest has surged in synthesizing faceted TiO_2 nanocrystals for photocatalytic activities.[91,159] For example, the use of high-energy {001}-faceted anatase TiO_2 has been well-studied in the degradation of dye pollutants, such as methylene blue and methyl orange.[160,161] More recently, however, the high {001} facet dependent activity has been questioned with evidence that the persistent fluorine on the nanostructures' surfaces resulting from HF used in the synthesis plays a non-negligible role on the photocatalytic activity, in fact enhancing it.[91,162,163] Because of

the strong fluorine bond, these fluorinated groups are not easily removed through washing or calcination. Therefore, HF-mediated syntheses of {001}-faceted TiO_2 often results in these groups remaining on the surface and obfuscating true facet-dependent behavior.

Cerium Oxide.—Ceria's effectiveness as a catalyst for organic degradation depends both on contaminant sorption ability as well as the Ce^{3+}/Ce^{4+} redox reaction efficiency to produce $HO^{\bullet}$. The reduction of Ce^{4+} to Ce^{3+} leaves behind V_os, and because the {100} and {110} facets of ceria have lower energies of V_o formation, these facets are more efficient in the recycling of the Ce^{3+}/Ce^{4+} redox cycle and thus catalyzing organic degradation.[31,103]

Regarding sorption of these organic contaminants on different ceria facets, Zang *et al.* found that the 6-fold coordination (Ce_{6c}) on the {110} and {100} facets exhibited stronger acidities and therefore stronger sorption of AO7 dye, compared with the 7-fold coordination (Ce_{7c}) on the {111} facet. However, the high sorption efficiency of the {110} and {100} facets were shown to be double-edged, as both facets also readily sorb high concentrations of H_2O_2, which can block active sites for contaminant sorption by forming surface-stable complexes. Additionally, Zang *et al.* noted that the oxygen-terminated {100} facet sterically hinders the adsorption of negatively charged AO7 dye, resulting in low degradation efficiency.[31]

A noteworthy consideration is that the Ce {100} polar surface is highly unstable. Though the ideal surface is oxygen-terminated, it is well-known that the surface is dynamic and different terminations (O, Ce, or a mixture) are possible, depending on synthetic and reaction conditions.[11] This maybe the reason that Zang *et al.*, who calcined their particles at high temperatures, observed different facet-dependent performance, {111} < {100} < {110}, than Majumder *et al.*, who did not report surfactant removal or post-treatment and observed {111} < {110} < {100}.[31,39]

Cuprous Oxide.—Cu_2O nanocrystals have consistently shown higher sorption capacity for methyl orange with increasing {111} and {110} terminations because of the higher exposure of Cu atoms on the surface and higher surface energy, compared to {100}.[110,112,164] The reactivity of the {110} facet is, however, complicated by the frequent coexposure of the inactive {100} facet.[99] Additionally, the {110} and {111} facets produce photoexcited electrons and holes more easily than the {100} facet due to saturated oxygen bonds.[164] With increased sorptive and redox capabilities, it is unsurprising that the {110} and {111} surfaces generally perform better as catalysts for organic degradation (Table 1).[99,107,164] However, Cu_2O particles are nearly completely inactive in the degradation of positively charged molecules such as methylene blue and methyl violet, likely because of the electrostatic repulsion between the positively charged contaminant and the copper-atom-terminated surface.[99,110] Further work investigating the efficacy of Cu_2O materials for degradation of neutral or positively charged molecules is needed to enhance the functionality of these materials for water treatment.

Hematite.—Hematite structures have been widely studied for their catalytic performance in photo-Fenton reactions because of the multitude of synthetic methods for nanostructures with well-defined facets. Generally, the undercoordinated Fe^{3+} atoms on the surface are the

sorption sites of dye molecules and the active sites of catalytic degradation. However, while the higher sorption efficiency of RhB on the {012} has been suggested to result from a higher density of unsaturated Fe ions, the studies did not consider the local coordination of the surface iron atoms.[113,114] In recent studies, the Fe-terminated {001} facet, dominated by a 3-fold undercoordinated iron (Fe_{3c}), was more active in degrading organic contaminants than the {012} facet, with primarily exposed singly undercoordinated iron (Fe_{5c}), despite the {012} facet having a higher density of undercoordinated iron.[72,113] This suggests that it is not simply the density of undercoordinated Fe but the *type* that aids in increased reactivity.

CO and Organic Molecule Oxidation.—As with Fenton-like reactions, the redox behavior of the surface metals is significant in the oxidation of CO and other molecules. CO oxidation typically takes place *via* a Mars–van Krevelen mechanism, where reactivity with sorbed and lattice oxygen (and the exchange between the two) is key (Figure 4).[11,122] Consequently, the ability of the NMO surface to store oxygen and facilitate transport of lattice oxygen to the surface is critical to CO oxidation, though these characteristics also apply to the oxidation of other organic molecules.[122] Additionally, the ability to sorb reactants and desorb products, largely dependent on the electron orbital energy match/overlap between the NMO and sorbent (see Mechanisms of Bonding Behavior), so as to not poison the catalytically active sites is critical.

Cerium Oxide.—Facile oxygen exchange as part of the Ce^{3+}/Ce^{4+} redox cycle is crucial to effective oxidation of CO to CO_2 on the CeO_2 surface, as is reviewed in detail elsewhere.[165,166] Because the {110} and {100} facets have lower V_o formation energies than the {111} surface, the {110}-terminated nanorods and {100}-terminated nanocubes have demonstrated higher performance in CO oxidation than {111}-terminated nanoparticles.[11,41,122] Jiang *et al.* demonstrated that ceria nanorods, coexposing the {100} and {110} facets, had a high density of surface V_os, resulting in effective propane and propene oxidation.[43] Interestingly, the two nanorod samples studied, differing only in the cerium salt precursor used during initial synthesis (cerium nitrate *vs.* cerium chloride), also possessed different densities of V_os.[43] Additionally, the high concentration of intrinsic defect sites on the {110} and {100} surfaces promote high oxygen mobility.[41] Due to their surface structures and short O–O coordination distances, {110} and {100} surfaces sorb CO in a strong bidentate fashion, whereas, on the {111} surface, weak binding occurs.[167]

Cobalt Oxide.—The Co^{3+} in the Co_3O_4 nanoparticles is regarded as the active site for CO oxidation, with the Co^{3+}/Co^{2+} redox cycle facilitating O adsorption and release.[168] The chemisorption of CO occurs at Co^{3+}, while Co^{2+} ions only sorb these species weakly, if at all.[169] Generally, the {100} facet is the least reactive and has the lowest proportion of exposed Co^{3+} atoms,[124,170–172] while the {110} surface has a high proportion of Co^{3+} exposed and is more catalytically active.[53,124,168,171–173] Cobalt nanorods preferentially exposing the {110} surface are found to exhibit excellent catalytic ability in CO oxidation, even in the presence of high levels of moisture and propane.[171]

However, discrepancies exist on the reported activity of the {111} facet. Some suggest that the {111} surface has no available Co^{3+}, making it inactive;[53,171,172] others note that there are sufficient Co^{3+} sites available.[124,168,173] Experimentally, the {111} facet

has been shown to be both active[126] and inactive[174] in methane combustion, and Wang *et al.* reported excellent catalytic decomposition of ammonium perchlorate on the {111} facet.[175] These discrepancies are likely explained by differences in experimental setup and pretreatment of the catalysts, as the polar {111} surface can be terminated by Co^{2+}, Co^{3+}, O^{2-}, or a mix, depending on experimental and synthetic conditions.[55] DFT calculations confirm that under various conditions (including water and H_2), the {111} can expose a variety of terminations.[55] Additionally, the atmosphere, temperature, and moisture content in pretreatment steps were empirically shown to have a large role on the catalytic activity of Co_3O_4 nanocrystals.[176] Reductive pretreatment of cobalt catalysts depressed catalytic activity, while moisture in the pretreatment gas stream caused water molecules to sorb and occupy catalytically active sites, decreasing the activity of the nanocrystals.[176] This supports another reported loss of activity in cobalt nanorods attributed to the accumulation of carbonate and water/hydroxyl species on the rod surfaces, blocking catalytically active sites for the adsorption of CO and oxygen.[171] As such, experimental studies need to explicitly report the pretreatment conditions to allow for direct comparisons between studies.

Cuprous Oxide.—The copper cations in Cu_2O materials are stable in multiple oxidation states and thus have a high ability to absorb and release surface lattice oxygen as they reduce and oxidize. Typically, the {111} and {110} surfaces outperform the {100} facet because the Cu atoms on these surfaces are exposed, and the exposed atoms on the {100} facet are coordinatively saturated.[130] Interestingly, Hua *et al.* found that although the {100} Cu_2O surface was more easily reduced than the {110} surface, the {100} surface was actually less active in catalyzing CO oxidation.[130] They suggested that this is because the {110} and {111} surfaces oxidize CO *via* a Langmuir–Hinshelwood mechanism, which primarily relies on adsorbed O rather than lattice O for the reaction to proceed. They also posit that the {100} surface is inert toward CO chemisorption when O-terminated. This contradicts the findings of Bao *et al.*, who suggest that CO binds very strongly onto the {100}-terminated surface to form a carbonate intermediate, which then decomposes *via* a Mars–van Krevelen mechanism.[131] While generally the order of catalytic performance follows {100} < {111} < {110} *(i.e.*, the inverse order of energy for V_o formation), Hua *et al.* reported the performance as {100} < {110} < {111} because they found that the {111} facet had the most unsaturated Cu(I) that were most active in chemisorbing CO (Table 2). The differences in performance may be due to the presence of organic surfactants for shape control of the crystals and incomplete or structure-altering removal methods.[177] Additionally, Wang *et al.* reported that, under high temperatures, the Cu_2O surface can oxidize to CuO, causing structural differences and non-equivalent comparisons across studies.[129]

In addition to CO oxidation, different facets of Cu_2O are capable of oxidizing propylene to different products, illustrating selectivity through intentional catalyst design.[132] Cubic particles that exposed mostly {100} facets combusted propylene to CO_2; octahedral particles that expose {111} facets partially oxidized propylene to acrolein; {110}-faceted rhombic-dodecahedral particles produced an almost equivalent mixture of propylene oxide, acrolein, and CO_2. The distribution of products depends on exposed atoms on the surface of Cu_2O, both in structure and type. On the {111} plane, the exposed singly coordinated Cu(I) was the active site; on the {100} plane, the exposed doubly coordinated O was the active

site; on the {110} plane, the triply coordinated O was the active site and responsible for the higher production of propylene oxide.[132] The results of this study suggest that selective, facet-dependent partial oxidation on the surface of NMOs is achievable, albeit understudied. Further work identifying similar product selectivity capabilities on the surface of other NMOs is essential for establishing robust structure–property–function capabilities for desired products realized through oxidative reactions.

Hematite.—Because of differences in surface structure, CO oxidation occurs *via* different mechanisms on the {110} and {012} compared with the {001} facet. Because the {110} and {012} surfaces primarily expose O surface layers, they cannot chemisorb atmospheric oxygen.[133] The CO oxidation pathway, therefore, proceeds by the Mars–van Krevelen mechanism (Figure 4). However, on the Fe-terminated {001} surface, CO and atmospheric oxygen chemisorb to the surface, forming a carbonate intermediate that decomposes to CO_2, a more inefficient reaction pathway.[133] This agrees with the work of Liu *et al.*, where higher densities of iron atoms on the {110} and {012} planes make them better sorbents of CO molecules, thus contributing to their higher activity.[135] Ouyang *et al.* also found that the order of CO chemisorption followed {001} < {113} < {012}, the same as the CO oxidation performance measured.[134] Additionally, although Hou *et al.* did not determine the exposed facets of their hematite nanostructures with different morphologies, they noted that the performance of CO oxidation followed the oxygen mobility (the propensity for oxygen exchange).[178] More robust studies on the V_o energies on each of the hematite facets are needed in order to confirm the higher activity of the {110} and {012} facets.

Water Splitting.—Splitting water is the critical pathway to produce hydrogen as a renewable fuel, where hydrogen is stored and then oxidized to release energy and regenerate water, resulting in a carbon-neutral energy production and consumption cycle.[179–181] Water splitting occurs through two fundamental half-reactions, the oxygen evolution reaction (OER) and the hydrogen evolution reaction (HER) (Figure 5a,b). Water splitting can be accomplished photocatalytically, thermally, or (photo)electrochemically, depending on where the energy for electronic excitation is derived. Since much attention has been paid to facet engineered electrochemical, photo catalytic, and photoelectrochemical (PEC) water splitting systems,[93,181,182] they will be the focus of this section.

Proton-exchange membrane or polymer-electrolyte membrane (PEM) and alkaline water electrolysis (AWE) are two promising ways of electrically splitting water. PEM and AWE are essentially inverses of one another, with PEM driven by OER at the anode producing protons, and AWE driven by HER at the cathode producing hydroxyl ions (Figure 5).[183] Both of these processes typically work best at either very high or very low pH, with the charge carrier (either H^+ or OH^-) concentration being very high.[181] However, electrochemical water splitting cells that are effective in mild pH environments are desirable to slow the rate of degradation of semiconductor electrodes and other cell components (*e.g.*, gaskets, connections).[181] Surendranath *et al.* demonstrated the possibility of utilizing cobalt-based catalysts as a thin film on the anode in neutral solutions, with numerous subsequent studies examining the OER activity of cobalt oxides.[184] It is important to note that, because of the physical separation between cathode and anode, charge recombination

is limited. Beyond the theoretical 1.23 eV minimum necessary to drive OER and HER, both processes require a significant additional energy, termed as “overpotential”, to proceed at appreciable rates.[181]

In photocatalytic water splitting, unlike electrochemical water splitting, the photogenerated electrons and holes are not physically separated and, instead, the quasiparticles are confined to the same photocatalytic particle, potentially leading to charge recombination before transferring to the desired surface adsorbate. This hinders the solar energy conversion efficiency and, thus, overall water splitting efficiency.[185] Additionally, because the electrons and holes simultaneously produce O_2 and H_2 on the surface of the photocatalyst, it is difficult to separate the desirable H_2 for fuel. In order for a single material to split water without a cocatalyst, its CB minimum must be at a more negative potential than the H^+/H_2 energy level, and its VB maximum must be more positive than the O_2/H_2O energy level.[179] It must have a band gap in excess of the theoretical minimum 1.23 eV energy necessary for water splitting to occur (though accounting for overpotentials and electron-transfer-induced losses, a much larger band gap is required).[181] Meeting these requirements is extremely difficult and has precluded the full scaled realization of overall water splitting.[185]

During PEC water splitting, a semiconductor absorbs photons that excite electrons from the VB to the unoccupied CB, generating excited electrons and holes. The excited electrons in the CB are transferred to the conductive substrate and then travel to the counter electrode through an external circuit, while the VB holes diffuse to the surface of the photoanode. The holes on the photoanode and the electrons on the counter electrode are then injected into the electrolyte to participate in OER and HER, respectively.[182] Since the pioneering work of Fujishima and Honda in 1972, TiO_2 has been the most well studied photocatalyst for light harvesting at the photoanode.[8,186,187] Notably, TiO_2 is a wide-band-gap semiconductor, meaning that it is inactive upon visible light irradiation, requiring energies of light in the UVA spectral range for an electron to be excited from the VB to the CB.[8] Though ultraviolet (UV) light has a higher energy than visible light, and thus is more efficient at generating hydrogen per photon, UV light accounts for only 4% of the total solar energy, necessitating a PEC system that can instead efficiently use visible wavelengths of light. Other limitations of the TiO_2 PEC system include the large overpotential in H_2 production on its surface, rapid reverse reaction between H_2 and O_2, and rapid recombination rate of photogenerated electron-hole pairs. Strategies such as the doping of noble metals and facet engineering have emerged as promising strategies to tackle these limitations.[8] As discussed above (see “Fenton and Fenton-like Catalysis”), the role of the exposed facet in improving TiO_2 photocatalytic efficiency is muddled by surface fluorine atoms, which also enhance water splitting performance.[188]

NMOs are well-studied as OER (photo)anode catalysts because of their reported high performance in other catalytic oxidative reactions.[181] In addition, most NMOs are studied as OER catalysts in basic media, where they are more resistant to dissolution (pH 13–14).[181] The OER reaction is often the rate determining half-reaction and is thermodynamically unfavorable because of the four-electron transfer, requiring a high-work-function catalyst to reduce the reaction energy barrier.[136] Improving the efficiency of OER by strategically tuning the design of NMO materials could enhance the water splitting mechanism

overall, as OER contributes to significant energy losses within the cell, caused by high overpotentials.[189,190]

The performance of an OER catalyst hinges primarily on its ability to sorb water or hydroxy molecules and to facilitate a proton-coupled electron transfer, as described above. The general mechanism of OER on metal oxides is shown in Figure 5.[189,191] Though RuO_2 and IrO_2 are well-known OER catalysts, these metal oxides are rare and costly.[191] For these reasons, the field of accessible OER/ORR catalysts is still receiving extensive research attention, presenting a crucial opportunity for researchers to fully capitalize on an enhanced structure–property–function understanding of NMOs. For example, excellent research has been done utilizing computational calculations and experimental observations to correlate surface reducibility, surface V_o formation, and O_2 binding energy with perovskite-based ORR electrocatalytic performance.[16,192]

Cobalt Oxide.—Co_3O_4 NMOs has been well-studied as electrocatalysts for OER in water splitting for their high performance, corrosion durability, and stable Co cations in multiple oxidation states, though bare Co_3O_4 NMOs are far less active and efficient than ones decorated on electroconductive materials such as graphene.[50] Possessing a low energy of V_o formation enhances adsorption of surface species (H_2O, OH), and subsequently their electron transfer for OER.[193,194] This is because the electrons neighboring the V_o become delocalized, making the surface more active for H_2O or OH^- adsorption.[195] Additionally, these delocalized electrons are more easily excited to the CB and increase the electrical conductivity of the electrochemical system.[194,195] The surface (hydr)oxo groups are important facilitators of Co-O intermediates that drive the OER reaction, and thus play important roles in the kinetics of this process.[196] With a high density of exposed Co^{2+} and Co^{3+} atoms on the surface[56] and low energy of V_o formation, the {111} facet is well-regarded as active toward water oxidation.[137,197] For example, Chen *et al.* note that on the {111} surface, water molecules dissociate to form Co-OH groups, which can be transformed into Co^{4+} oxo sites during OER that can subsequently form hydroperoxide and other intermediates to start the water oxidation cycle.[56] The {110} facet has also been shown to perform well as an OER catalyst.[50,136,198] Conversely, the {100} facet has poor performance,[50,56,136,198] because of its low density of exposed Co^{2+}, thought to be the active site for OER.[50,56,136]

However, the active site of Co_3O_4 OER is controversial, with some reports showing the octahedral Co^{3+} site as being the most active for OER,[50,197,198–200] and others demonstrating that the tetrahedral Co^{2+} site is the active site for OER.[56,136,201] To resolve these discrepancies, Wang *et al.* undertook a systematic investigation to identify the roles of Co^{2+} and Co^{3+} in OER by substituting them in the Co_3O_4 structure with Zn^{2+} and Al^{3+}, respectively. These results revealed that both ions were differently responsible for OER but that Co^{2+} sites were far more active and able to facilitate the formation of CoOOH, the main active site for OER. They note, however, the synergistic effect of both Co^{2+} and Co^{3+} in OER efficiency.[201] These results suggest that utilizing facets with a high density of Co^{2+} active sites, such as {111} and {110}, may optimize the efficiency of Co_3O_4 catalysts in water splitting, but a more definitive elucidation of the active sites for OER/ORR is necessary to investigate this fully.

Hematite.—Hematite has emerged as a promising material for light-driven OER in photoelectrochemical water splitting.[202] For these reactions, surface OH species have been shown to actively participate in water oxidation. Though facet-dependent performance studies are nascent, a recent study of the {001}, {012}, and {104} hematite surface for water oxidation demonstrated that the {012} surface performed exceptionally well as a catalyst for OER.[139] This is because the surface adsorption of the oxygen intermediates (HO* and O*) on the {104} surface is too weak, while on the {110} it is too strong (and significant energy is therefore required to desorb and form the final O_2 product). Although this suggests that the {012} surface is a promising facet to catalyze OER activity, Li *et al.* thoroughly investigated the kinetics of OER on {012}- and {001}-faceted hematite nanostructures and found that despite it being a more active transferer of electrons to the H_2O reactant, the {012} facet is also more active in charge recombination. This is because while the {012} facet has a higher density of surface OH species, it also has a higher density of surface states (energy levels between the CBs and VBs), resulting in less charge separation between electrons and holes. More efficient electron transfer and charge recombination are consequently enabled, limiting the overall efficiency of water oxidation. It would therefore be highly beneficial to develop a catalyst that improves charge transfer kinetics from the active surface sites but does not promote recombination.[138]

Hydrogenation.—Unlike oxidative reactions, hydrogenation of organic contaminants takes advantage of surface oxygens as stabilizers for reactive organic molecules, with CeO_2 being most studied. Interestingly, ceria's "stable" {111} surface performs best, followed by {100} and {110} (Table 1).[141–143,203,204] Because the {111} surface possesses a lower capacity for V_os, and nearby oxygens act as stabilizers of reactive hydroxyl intermediates, the production of oxidized compounds is prevented and the hydrogenation reaction is progressed.[11,141–143] However, the product selectivity in the semihydrogenation of propyne is limited due to the presence of surface oxygen atoms that inhibit the transition state geometry.[143] Further studies of hydrogenation over other NMO catalysts are needed to comprehensively establish this proposed inverse trend to oxidative reactions.

Organocatalysis.—Unlike reactions occurring in oxidative or reducing environments, V_os are relatively unimportant for organocatalysis, as it does not depend on the redox chemistry necessary in oxidative reactions. Rather, these processes are surface facet dependent because of the availability of various sites for complexation with reactants. On the surface of Cu_2O, where this phenomenon is most studied, the availability of the copper atoms is essential for synthetic reactions, facilitating the formation of bonds between the Cu_2O surface and the organic reactants and allowing for efficient formation of the final product.[145,146] The {110} surface fully exposes Cu atoms and performs the best, followed by the {111} facet, where the Cu atoms are partially blocked by surface oxygen atoms, and last the {100} plane because the Cu is only partially exposed.[146] This pattern of {100} < {111} < {110} was found to be the case in the [3 + 2] cycloaddition reaction for the generation of 3,5-disubstituted isoxazoles, the synthesis of 1,2,3-triazoles, and in the N-arylation of iodobenzene with imidazole to synthesize 1-phenylimidazole (Table 1).[145–147] All three studies demonstrate remarkable (regio)selectivity, indicating Cu_2O nanomaterials could be useful as selective catalysts in future synthetic reactions. Further work to determine the

selective catalytic capabilities of other NMOs in other synthetic reactions is needed to determine if this ability is unique to copper oxides and azole compounds.

Informed Design for Catalysis.—From these facet-dependent studies of different NMOs catalysts, these general takeaways are identified as key for high reactivity or enhanced catalytic activity:

Catalytic Oxidation.

1. easily reducible (*i.e.,* at reasonable temperatures and oxygen partial pressures) surface metal ions
2. high mobility of oxygens and oxygen vacancies (V_os) between bulk and surface
3. high densities of V_os and low energies of V_o formation since they make high-energy electrons available in the CB enabling more effective catalytic oxidation for a variety of reasons (higher production of ROS; stronger binding of adsorbates/reactants and assistance in their dissociation; modification of electronic band structures)
4. facets with exposed and undercoordinated metal cations to enhance electron transfer
5. facets terminated by metals (rather than oxygen atoms) to complex more readily with H_2O_2 and target contaminants, facilitating enhanced degradation (although, H_2O_2 can also act as a competitor for contaminant sorption sites)
6. facet engineering to induce modified band gap energies and positions, so NMOs can be tuned to have a smaller band gap (increasing solar light absorption efficiency) or a larger band gap (to produce charge pairs that efficiently oxidize water)

Hydrogenation.: Facets with low oxygen vacancy capacity facets.

Organocatalysis.: Facets with high availability of metal active sites (does not rely on V_os).

For all catalytic reactions, the most effective catalysts are ones that bind atoms and molecules with an intermediate strength such that the reactants are activated but the products desorb (following the Sabatier principle)

Gas Sensing.

Semiconductor metal oxide (SMOX) gas sensors, in general, detect the presence of a gas through a change in electrical signal (*i.e.,* resistance).This overall process is broken down into two basic processes: reception, which includes the sorption of the target gas and the exchange of electrons with the SMOX surface; and transduction, which involves the translation of the surface reaction into measurable electrical signals.[205,206] This section will focus on the reception process, as it is analogous with the sorption-based processes described throughout this work.

The adsorption/desorption model of the reception process is based on the supposition that chemi-/physisorption of oxygen and target gases results in a change in resistance due to a change in charge carrier concentration. It is the most robust and well-developed model for gas sensing and will therefore be the focus of this section (Figure 6).[207] This section will focus on the oxygen ionosorption model, whereby chemisorbed oxygen and target reducing/oxidizing gases are the main active species because this model more accurately describes sensors under normal atmospheric conditions.[208] However, lattice oxygen can also participate in surface reactions, though the interaction between reducing gases and this lattice oxygen has a larger energy barrier than chemisorbed oxygen.[209] The energy required to break the metal–oxygen bond for desorption of the sensed gas is therefore higher, resulting in a slow sensor recovery time or a necessarily higher operating temperature that may change the structure of the SMOX and be infeasible for detecting flammable/explosive gases.[210]

There are two types of SMOX gas sensors: n-type and p-type (Figure 6). n-type sensors have a band structure with electron energy levels near the top of the band gap (*i.e.*, a Fermi level near the CB), and thus electrons (the majority carriers for current flow) can easily be excited from the VB to the CB (Figure 6a).[211] p-type sensors, mechanistically inverse to the n-type, have a structure such that unoccupied states exist in the band gap just above the VB (*i.e.*, near the Fermi level), and electrons can be elevated from the VB to the band gap states, leaving holes (the majority carriers for current flow) in the VB (Figure 6b).[211] It is worth noting that gas sensor nanoheterostructures, materials comprised of a combination of n- and/or p-type SMOXs that have been documented to increase sensor performance due to unique electronic effects and interfacial interactions, also present extensive opportunities to develop a robust structure–property–function relationship but are not detailed here because of the immense diversity of structure and materials available.[212] For both types of SMOX gas sensors, target gases are sensed on the basis of a change in resistance that occurs because of the interaction and exchange of electrons between the target gas and adsorbed oxygen species on the surface of the NMO material.[210] For this reason, chemisorption of target gases is essential, while physisorption elicits almost no response.[208]

The n-type SMOX gas sensors (*e.g.*, ZnO, SnO_2, Fe_2O_3, and CeO_2) are the most commonly studied because of their higher sensitivity toward trace concentration of reducing gases due to the significant variation in chemiresistivity at the site of molecule adsorption.[210,211] p-type semiconductors, including Co_3O_4 and Cu_2O, have received less attention because of their lower sensitivity, with Hübner *et al.* reporting that the gas response of p-type oxide semiconductors is equal to the square root of the morphologically identical n-type NMOs.[3,211,213] This is because, with the reasonable assumption that oxide semiconductor particles are larger than twice the thickness of the hole accumulation layer (HAL), the concentration of holes in the shell layer due to electron–hole recombination after the adsorption of target gases does not lead to a significant variation of chemiresistivity.[211,213] So, while the sensitivity is far lower, p-type semiconductor sensors do not suffer from the same humidity impedance as n-type semiconducting sensors.[211]

Because both n- and p-type semiconductor sensors measure changes in resistance upon sorption and reaction between target gases and oxygen species, a semiconductor facet that

promotes the chemisorption of oxygen should make a high-performing and sensitive SMOX gas sensor.[208,210] Specifically, NMO facets with a high electron density in the CB are more readily able to transfer electrons to the oxygen adsorbate to form a bond (see Mechanisms of Bonding Behavior). In addition, because oxygen vacancies serve both as direct adsorption sites and electron donor sites, a higher density of V_os is a major advantage for effective SMOX gas sensors.[206] Though this is a simplistic description of the role of V_os (see excellent recent review distinguishing the role of surface and bulk V_o and evaluating the role of additional confounding factors[208]), it is generally accepted that V_os play a crucial role in dictating the sensitivity of a SMOX gas sensor, even when assuming a surface ionosorption-based mechanism.[208,210,214] For example, a high concentration of V_os has been shown to enhance alcohol adsorption and dehydration product desorption, both necessary steps in the sensing and regeneration of metal oxide gas sensors.[215] As will become relevant in the subsequent discussion, both oxygen vacancy defects and metal dangling bonds are functionally equivalent in that they both promote enhanced sorption on the sensor surface.[216] These considerations are very similar to those described for catalysis, and it is therefore unsurprising that effective catalysts are often effective in SMOX gas sensing applications. However, although the ability to desorb oxygen and oxygen intermediates aid in the regeneration of active sites and accelerate the recovery time of the gas sensor, the absolute performance and sensitivity are less dictated by this ability than catalysts because SMOX gas sensors rely primarily on charge transfer and changes in resistivity.

n-Type Gas Sensors. Hematite.—Though morphology-dependent hematite gas sensing performance has been studied,[134,217,224,225] few directly compare facet performance of low-index nanostructures. Ouyang *et al.* studied the sensing ability of hematite nanostructures toward acetone and found that the {001} facet underperformed in comparison with the {012}- and {113}-faceted structures because of a low density of undercoordinated Fe atoms at the surface, which can facilitate more oxygen sorption for higher sensitivity.[134] Gao and Zhang calculated the density of dangling bonds on hematite facets and confirmed that the {012} facet has a higher density of dangling bonds than the {001} facet, meaning that it will likely be the highest performing low-index facet (though they did not perform calculations for {110}).[3]

Tin Oxide.—Most studies of facet-dependent SnO_2 performance focus on its capacity as a gas sensor. The most commonly studied surfaces in this respect are {110}, {101}, {111}, {221}, and {332}, with the latter two surfaces being high-index and high-energy. The trend of having more undercoordinated Sn^{4+} atoms leading to higher performance is generally followed, as this facilitates more oxygen adsorption and higher sensitivity.[3] Wang *et al.* note that the {221} surface, which performed worse than {111} for CO oxidation, actually performs better than the {111} facet in ethanol sensing capabilities.[85] This is because, in catalyzing CO oxidation, the stepped surface and higher Lewis basicity of the {221} facet made it difficult for the CO_2 product to desorb, thus leading to the poisoning of the active sites. However, the stepped {221} facet was actually more active in the adsorption of the ionized oxygen species and thus showed a higher sensitivity toward ethanol sensing.[85] It is important to note, however, that this study did not detail the mechanisms of oxygen or

ethanol desorption from SnO_2 structures, which will undoubtedly have an effect on the recovery and practicality of these sensors.

Zinc Oxide.—ZnO has been a well-studied NMO for gas sensing, and, as with other NMO gas sensors, its facets with a high proportion of oxygen vacancies significantly enhance oxygen adsorption, leading to higher sensitivity. Han *et al.* noted that the Zn-terminated {001} surface was best at adsorbing atmospheric oxygen because the surface Zn atoms were coordinatively unsaturated, compared with the mixed-termination {100} surface and the relatively inert O-terminated {101} surface, which could not sorb oxygen species because of the inability of surface O^{2-} to sorb oxygen.[220] The findings of Zhao *et al.* support this, showing that the polar Zn-terminated {001} planes performed better as a gas sensor than nonpolar {010} facets, because {001} has more oxygen vacancies.[219] The activity of the {001} facet is further corroborated by Xu *et al.*, who used DFT calculations to show that the {001} facet sorbed O_2 more strongly than the {100} facet, explaining the higher performance of the {001} nanosheets over {100} nanosheets in ethanol sensing.[216] Kaneti *et al.* also found that the {001} nanoplates outperformed the {100} nanorods in sensing ethanol, due to an enhanced adsorption capacity, but noted that because of this higher affinity (stronger interaction), the recovery time of the nanoplate sensors was slightly longer than that of the nanorods.[221]

p-Type Gas Sensors. Cobalt Oxide.—Very few studies exist on the facet-dependent capabilities of Co_3O_4 structures. Only one, by Zhou and Zeng, suggests that the {111} surface is more active than the {100} surface in sensing methanol, ammonia, ethanol, and acetone, likely because, as noted with catalytic studies, the {100} facet has the lowest proportion of exposed Co^{3+} sites, which are generally regarded as the most active.[222] More robust studies on the performance of Co_3O_4 particularly in gas sensing would aid in elucidating these mechanistic suppositions.

Cuprous Oxide.—Despite its wide attention as a catalyst, Cu_2O has not been well-studied for facet-dependent gas sensing capabilities. Wang *et al.* showed that {111}-octahedra outperformed {100}-cubes in sensing CO, despite having a lower surface area. The {111} surface, terminated by both Cu and O atoms, has a higher density of exposed, coordinatively unsaturated Cu atoms, making it a better performing gas sensor, while the {100} facet is terminated by O atoms that do not interact with ionized oxygen species necessary for gas sensing.[223] Gao and Zhang, however, utilized computational calculations to show that the {110} facet contains a higher density of undercoordinated Cu atoms, and would likely perform superiorly to the {111} facet, as observed in its catalytic performance.[3] Experimental evidence to support this hypothesis is needed.

Informed Design for Gas Sensing.—As with catalysis, understanding the structure of the NMO will be essential for the informed design of efficient gas sensors. Particularly because NMOs are generally understudied as gas sensing materials, this represents an opportunity within the field to comprehensively integrate structure–property–function understandings into experimental studies, rather than a *post hoc* justification of enhanced performance. The following conclusions can be gleaned from the current literature on

facet-dependent NMO sensing performance as well as analogous inferences from catalysis studies detailed above:

1. The ability to adsorb atmospheric oxygen species and target molecules is crucial for enhanced sensitivity.
2. A high surface accessibility of undercoordinated metal atoms and steps leads to higher sensitivity.
3. A large number of V_os and a low energy of V_o formation may enhance the oxygen and other target gas sorption capabilities of the gas sensor, thus increasing the overall performance.

Because the mechanisms of gas sensing are similar to those of catalysis, it is likely that the performance trends will be similar but should be validated empirically and computationally. More research is necessary to reach informed design of gas sensors with the following questions still remaining to be investigated:

1. further investigation of p-type semiconductor facet-dependent gas sensing performance to ascertain whether exposing certain facets can aid in overcoming their historically low sensitivity
2. pursual of whether the *type* of coordination in addition to the density of undercoordinated metal atoms affects performance (as in catalysis)
3. discernment between the effects of surface and bulk oxygen vacancies on gas sensing sensitivity
4. design efforts to reduce the impeding effect of humidity on the sensitivity of gas sensors, perhaps utilizing facet design to minimize the competitive sorption of water molecules on active sites
5. design efforts to improve selectivity capabilities of gas sensors to target molecules of concern
6. design efforts to increase effective desorption of sensed gases so as to reduce recovery times, particularly at low temperatures

Contaminant Sorption.

Compared with catalysis, facet-dependent studies focused on direct sorption and removal of aquatic contaminants are relatively sparse, with studies on NMOs for these applications being even more limited (Table 3). For this reason, this section will draw upon facet-dependent sorption studies of non-nanoscale metal oxides as well as more recent work on NMO sorption behavior to draw inferences about how a structural understanding of NMO materials can aid in the development of next-generation sorbents.

In aqueous solution, any unsaturated bonds or oxygen vacancies are filled by either OH^- or H_2O ligands, and these surface groups, and their exchange, largely dictate NMO performance in the removal of target contaminants.[226] Typically, the surface hydroxyl groups first facilitate a weak outer-sphere complex with the contaminant through electrostatic interactions and an extensive hydrogen bonding network. These surface groups

can then undergo a ligand exchange with the contaminant to create an oxygen bridge and form an inner-sphere complex.[10,74] Depending on the number of oxygen bridges formed and the number of metal centers involved, direct sorption can be classed as either monodentate mononuclear, bidentate mononuclear, bidentate binuclear, or, albeit rarely, tridentate (Figure 7).[10] The most effective NMO sorbents possess exchangeable OH^- or OH_2 groups and facets with a high density of these exposed groups. Additionally, the pH, ionic strength, and redox potential of solution play a large role in the speciation of the target contaminants and their ability to adsorb to a metal oxide surface (Table 3, "Note").[227] Furthermore, because these species are typically charged at environmentally relevant pHs, the point of zero charge of the NMO surface impacts the efficiency of removal. The presence of competing species, always present in natural water systems, also plays a large role in the adsorption kinetics and thermodynamics, and thus the development of selective adsorbents is highly desirable (see Future Directions and Opportunities).

With distinct orientations of available surface atoms and unique electron densities for the formation of bonds, it is unsurprising that different facets behave differently as sorbents. One of the first thoroughly investigated facet-dependent sorption studies was by Bargar *et al.*, who utilized X-ray spectroscopy to investigate Pb^{2+} adsorption on non-nano corundum (α-Al_2O_3).[226] On the {001} facet, the ions bind in an outer-sphere configuration, but on the {012} facet, they bind in a stronger inner-sphere conformation despite the {012} surface having a lower density of hydroxyl groups (thought to be the active sorption sites). However, the {001} surface possesses predominately doubly coordinated hydroxyl groups, whereas the {012} surface has mostly singly and triply coordinated hydroxyl groups. These singly and triply coordinated groups were shown to be much stronger Bronsted acids, whereas the doubly coordinated groups are weak acids, very stable, and thus less likely to exchange.[226]

On isostructural hematite, these doubly coordinated groups are similarly difficult to exchange because simply removing the H atoms leaves a dangling double oxygen bond, while removing the entire OH group breaks two Fe–O bonds. Both of these scenarios are much more energetically unfavorable than removing the H atom from a triply coordinated hydroxyl group to form a dangling single oxygen bond or removing the OH group from a singly coordinated hydroxyl group to break only one Fe–O bond.[79] The labile exchange of singly coordinated hydroxyl groups has also been seen in the sorption behavior of arsenate and phosphate on goethite (FeO(OH)).[228] Clearly, the density and coordination type of exposed hydroxyl groups play a large role in the ability of a metal oxide to sorb contaminants with additional evidence that coordination structure contributes to sorption behavior.

Hematite.—The different facets of hematite have different densities of singly, doubly, and triply coordinated hydroxo groups.[79,243,244] Barron and Torrent calculated the density and type of hydroxyl groups on each of the low-index surfaces of hematite and showed that {001} possessed only doubly coordinated groups, {110} possessed equal amounts of singly, doubly, and triply coordinated groups, and {012} possessed mostly singly and triply coordinated groups.[243] These different surface groups also have different proton affinities,[244,245] as well as kinetics of proton exchange.[246] Singly and triply coordinated oxygen surface groups promote much more favorable exchange behavior and, thus, serve as

active sites for contaminant sorption. Accordingly, the {012} and {110} facets of hematite have much stronger adsorption affinities and higher capacities for contaminants of concern (Table 3). For example, Catalano *et al.* have reported the preference of arsenate (As(Vl)) and selenite (Se(lV)) to bind to singly and triply coordinated oxygen functional groups because of favorable sterics, kinetics, and acidities.[69,247] Noerpel *et al.* used resonant anomalous X-ray reflectivity (RAXR) to determine the surface coverages of Pb^{2+} sorbed on various hematite facets and similarly showed that the {012} and {110} facets (with higher densities of singly and triply coordinated hydroxyl groups than {001}) had a higher surface coverage of Pb^{2+} per surface area.[76] The higher density of singly coordinated hydroxyl groups on the {100} surface of hematite was also shown to be responsible for the greater sorption capacity (per surface area) of humic substances compared with the {001} facet,[235] with analogous conclusions for enhanced sorption and subsequent hydrolysis of 4-nitrophenyl phosphate on the {100} vs. {001} facet of nanohematite.[238]

In addition to relative differences in sorption capacities, recent research has demonstrated that different facets of nanoscale hematite also promote different complexation geometries for both inorganic and organic contaminants. For example, Huang *et al.* showed that chromate bound *via* a monodentate, mononuclear complex on the {001} facet, but on the {110} facet bound as a bidentate, binuclear complex, and was removed with much greater efficiency.[67] Lounsbury *et al.* showed that selenite sorbed in a bidentate binuclear geometry on the {110} facet, promoting stronger adsorption, compared with the bidentate mononuclear geometry on the {012} facet.[233] Additionally, Cao *et al.* demonstrated that phenylarsonic acid formed a bidentate binuclear complex on the {012} facet and a monodentate mononuclear configuration on the {001} surface, and that the lower adsorption energy for the formation of the bidentate nuclear complex resulted in a higher adsorption capacity on the {012} surface compared with the {001} surface.[81] These differences in binding geometries are derived from differences in surface structure and atomic arrangement, impacting the available atoms and bonding distances for the formation of each complex.

However, before drawing conclusions about facet-dependent sorption behavior, it is important to note that the hydroxyl densities change depending on which surface termination of hematite is being considered. As described in Atomic and Electronic Characteristics of NMO Facets above, many terminations of hematite facets are possible depending on material preparation and experimental conditions. The importance of integrating surface science with direct sorption experiments was underscored by a recent publication by Qiu *et al.*, who studied lead sorption on the full-termination {012} facet of cut and polished hematite.[74] In a prior study, the same research group found that, on the half-layer termination, Pb^{2+} bound at two distinct FeO_6 octahedral edges to form two different bidentate, edge-sharing structures.[73] However, on the full-layer termination, only one of these structures was found because the reorientation of Fe and O in the half-layer termination meant that the binding geometry (*i.e.*, bond angles and lengths) of the second structure were too energetically unfavorable.[74] That surface structures with subtle differences influence the availability of sorbate complexation sites highlights the importance of integrating an understanding of NMO surface structure with the thermodynamics of binding geometries and the sorption behavior of contaminants across different NMO facets.

Titanium Dioxide.—Because of its photocatalytic capabilities, anatase TiO_2 has been studied for sorption and photooxidation/photoreduction of inorganic contaminants, including arsenic, antimony, and uranium.[240–242] For all of these studies, the sorption of the target metal was highest on the {001} facet, leading to enhanced photodegradation behavior. Notably, however, HF acid was used during the synthesis of the {001}-faceted TiO_2 and, as discussed previously, this likely enhanced the reactivity of the particles.

Informed Design for Contaminant Sorption.—Facet-dependent sorption performance is understudied, particularly for NMOs. It is therefore difficult to definitively determine which facet(s) would promote enhanced or selective sorption since nanomaterials possess unique structural and electronic characteristics that will undoubtedly change their sorption behavior compared with bulk crystals.[1,248] However, the following inquiries could aid in the pursuit of understanding the structure–property–function relationship for contaminant sorption:

1. structural characterization of NMOs and NMO–contaminant complexes to ascribe and understand true facet-dependent sorption behavior
2. determination of whether singly and triply coordinated (hydr)oxo groups, and facets that expose a high density of these groups, facilitate facile contaminant sorption on a broad suite of NMO sorbents
3. utilization of DFT calculations with appropriate environments (*e.g.*, including solvation) to screen NMO facets that have favorable bonding capabilities with target sorbates and promote stable contaminant complexation geometries to reduce the number of experimental studies need
4. investigation of the effect of faceted NMO aggregation and surface complexation in aqueous solutions on sorption behavior
5. experimental work in mixed water systems with multiple different competing sorbates to observe impacts on facet-dependent behavior as it remains to be seen whether facet engineering can yield selectivity capabilities and improve overall performance

EXTENSIONS OF FACET REACTIVITY

Many opportunities exist within the realm of facet-engineering and nanostructure-informed design that are currently being explored to increase the reactivity and efficiency of NMOs in different applications. Design of advanced NMO-based materials can capitalize on the basic structural understandings that have been examined by the work detailed in this review as well as additional synergistic interactions. The case studies presented herein underscore the importance of considering the unique atomic and electronic structures of each individual component as well as their interdependent interactions when evaluating facet-dependent performance of hybrid materials. These sections are not intended to be comprehensive in scope but rather demonstrative case studies to incite further discussion about how to incorporate facet-dependent reactivity in the design of more complex materials.

Synergistic Metal–Metal Oxide Support Interactions.

Metal oxides have been studied as support structures for metal particles, often enhancing the performance capabilities through synergistic interactions. For example with nanostructured ceria supports, the electronic state of the deposited metal particles has been shown to depend on the ceria facet: on {100} facets the metal is slightly negative, but on the {111} facet the metal exhibits a slightly positive oxidation state because of differences in V_os.[11]

Copper-ceria materials have been intensely investigated because of the synergistic effect between the Cu^{2+}/Cu^{1+} and Ce^{3+}/Ce^{4+} redox cycles. Wang *et al.* showed that Cu atoms adsorbed on the {111} ceria facet were dispersed as CuO_x but on the {110} ceria facet they were strongly bound as Cu–[O_x]–Ce species.[249] The CuO_x clusters were much more easily reduced to Cu(I) active sites upon exposure to CO because of weak interactions between CuO_x and {111}-CeO_2 compared with the Cu–[O_x]–Ce species, which were strongly bound and inhibitive of CO oxidation. This mixed-metal oxide demonstrated opposite facet dependence to pure CeO_2 materials: here {111}-faceted ceria outperformed {110}.

Hu *et al.* studied Pd-ceria materials in CO and propane oxidation.[250] Similar to the Cu–Ce materials described above, Pd–O–Ce linkages were found on the {110}-rods and {100}-cubes, and PdO_x species predominated on the {l1l}-octahedra. Unlike Cu–Ce, the Pd metal on the {110}- and {100}-faceted nanorods showed the best performance in CO oxidation, attributed to its high reducibility. However, for propane oxidation, the {111}-faceted octahedra had high catalytic performance since PdO_x dominated and the Ce–O bonds were less relaxing so the carboxylates were unstable. This led to the conclusion that surface oxygen mobility is not as crucial for propane oxidation as the chemical adsorption and activation.[250]

Synergistic Mixed-Metal Oxide Support Interactions.

Mixed-metal-oxide support-structure materials are being increasingly studied for the selective catalytic reduction (SCR) of NO_x gases with NH_3 as the reducer (NH_3–SCR), recently demonstrating potential benefits of facet engineering.[251,252] The application of NMOs in NH_3–SCR has historically been limited by impedances from coexisting gases (*e.g.*, SO_2 and H_2O vapor) in the flue gas and the poor low-temperature operating ability (optimal performance typically 300–400 °C).[251] With mixed NMOs, Han *et al.* showed that Fe_2O_3 embedded on the surface of faceted CeO_2 nanostructures outperformed bare CeO_2 by having much stronger adsorption of NO and NH_3, lower reduction temperature, and enhanced redox properties.[251] Additionally, the {110}-/{100}-faceted ceria of the Fe_2O_3/CeO_2 nanorods outperformed the {111}-/{110}-faceted ceria of the Fe_2O_3/CeO_2 nanoparticles. This enhanced performance is linked to nanorods having a higher concentration of oxygen defects, thus providing a higher density of active sites to adsorb O_2 for facile redox NO–NH_3 reactions. Additionally, the nanorods were less affected by SO_2 gas and H_2O vapor and oxidized ammonia to a lesser extent (meaning that more NH_3 was available to facilitate NO_x reduction), with a high degree of N_2 selectivity.[251] Relatedly, Liu *et al.* also showed that {001}-faceted Fe_2O_3/anatase-TiO_2 nanosheets outperformed {101}-faceted Fe_2O_3/anatase-TiO_2 nanospindles in the same NH_3–SCR, with results nearly mirroring that of Fe_2O_3/CeO_2. The {001}-faceted Fe_2O_3/TiO_2 nanosheets had a higher

density of surface-adsorbed oxygen (related to its density of surface oxygen defects), more acid sites, and more easily facilitated regenerable Fe redox chemistry. The {001}-faceted nanosheets (both bare and with Fe_2O_3) demonstrated superior adsorption of NH_3 and NO_x and desorption of nitrite and nitrate species compared with the {101}-faceted nanospindles.[252]

Yao *et al.* also studied the impact of metal oxide support structures in NH_3–SCR by comparing MnO_x embedded on SiO_2, TiO_2, CeO_2, and γ-Al_2O_3. Each of these support structures demonstrated different MnO_x dispersion, reduction behavior, surface acidity sites, and adsorption–desorption behavior, each of which contributes to the overall NH_3–SCR reaction. Despite having the best reduction behavior, the CeO_2/MnO_x structure did not perform best overall because its nonselective oxidation of NH_3 (the reducing agent) in addition to its reduction of NO_x limited the overall catalytic activity. In fact, the MnO_x/γ-Al_2O_3 material performed best because of a combination of good MnO_x dispersion, sufficient reduction behavior, high density of acid sites, excellent NO_x adsorption, abundant Mn^{4+} exposure, and complete reduction of NO to N_2. Its catalytic performance, however, was significantly impeded by the presence of SO_2 and H_2O.[253]

Synergistic Facet Interactions.

Because most nanoparticles coexpose multiple facets, it is critical to understand the synergistic/antagonistic interactions between these facets. Additionally, interactions could present excellent opportunities to increase the effectiveness of NMOs without needing support structures or mixed materials. For example, effective pollutant degradation has been achieved with a near-equal percentage of exposed {001} and {101} TiO_2-anatase facets compared with single-faceted anatase nanostructures. This is because the {001} facets have a high concentration of O centers (oxidation sites), while {101} facets have more Ti centers (reductive sites).[254] Since the VB of the {001} facet extends to higher energies than the {101} facet, but the CB remains in a similar position, holes and electrons are free to migrate to realize the most stable energy configuration.[8] In other words, having a mixture of {001} and {101} facets can form a heterojunction where photogenerated electrons migrate to the {101} facet and photogenerated holes migrate to the {001} site.[255] While the {001} facets were indeed shown to be more active for oxidation, Roy *et al.* showed that having a near-equal mixture of both sites prevented recombination of holes and electrons, making TiO_2 more efficient at degrading methyl orange dyes.[256] Similar excellent results were seen in using N-doped TiO_2 nanobelts for photocatalytic water splitting. While the N-dopants lowered the TiO_2 band gap, increasing the percentage of visible light viable for electron excitation, the coexposed {001} and {101} facets segregated the photogenerated holes and electrons, minimizing the charge recombination.[257]

CONFOUNDING FACTORS

While efforts have been made to understand the reactive behavior of different NMO facets in many environmental applications, several studies report conflicting conclusions in terms of identifying the preferred reactive NMO facets, often due to differences in synthesis methods and experimental setup.

It has been widely reported that surface-directing agents used to controllably expose NMO facets occupy active sorption sites, thus veiling true facet-dependent properties and performance.[177,258] This is especially pertinent in the synthesis of TiO_2 nanostructures, where fluorine is often used to expose high-energy {001} facets.[158] Residual fluorine on the surface of these nanostructures has a significant effect on photocatalytic activity, oftentimes muddling the elucidation of the true reactivity of the {001} facet.[91,163] However, even for less harsh ligands such as organic capping agents such as oleic acid and poly(vinylpyrrolidone), enhanced and diminished catalytic behavior has been reported.[177] It is therefore imperative that researchers investigating facet-dependent performance thoroughly detail their synthetic methodology and meticulously demonstrate the removal of residual surface ligands or quantify their impact on sorption/catalytic behavior before any performance is measured. Further investigation into synthetic methods that produce uniform faceted NMOs are necessary to resolve some of these discrepancies.

Additionally, appropriate material characterizations to ensure analogous comparisons across studies are essential. Normalization by surface area or active site, rather than mass, especially in sorption isotherms, will more accurately account for the active components contributing to facet reactivity. However, surface area measurements must also be accompanied by additional measurements and discussion of surface structure and the availability of active sites, as not all Brunauer–Emmett–Teller surface areas are available for complexation (especially small micropores).[10] Additionally, it is essential that nanomaterials designed for use in water treatment applications also be evaluated for their aggregation behavior, which is well-known to occur in aqueous solutions and can affect sorption of target contaminants.[259,260] Higher energy (and, thus, more reactive) facets, in particular, will tend to aggregate in order to reduce surface energies, so quantification of this aggregation behavior will be necessary to clarify true facet-reactive behavior.[261]

Finally, variation in experimental environments can consequently induce significant structural changes to NMO surfaces, resulting in a large impact on facet-dependent behavior. Many studies, particularly on very reactive (read: unstable) facets, do not take these changes into consideration but are well-documented under different oxidizing and reducing conditions, different temperatures, humidity conditions, and postsynthesis annealing.[44, 61,63,262] This alters the termination and exposure of surface atoms, thus impacting the characterization and comparison of NMO facet performance. In order to assuredly compare different NMO facets in environmental applications across studies, emphasis on these experimental conditions and the resulting change on surface structure should be thoroughly detailed (see Future Directions and Opportunities).

FUTURE DIRECTIONS AND OPPORTUNITIES

In this review, we have presented the importance of developing a rigorous understanding of the structural and electronic factors essential for enhanced material performance in three key environmental applications: catalysis, gas sensing, and direct sorption of aquatic chemical species. We have coupled this understanding with a discussion about how facet engineering has been shown to improve the efficiency of accessible NMO materials through controlled exposure of active surface sites. Although this burgeoning field has made

significant progress, we highlight the continued need to integrate a robust understanding of surface structure with performance-based studies. Designing materials specifically for particular applications, rather than justifying their performance *a posteriori*, represents a necessary shift in the informed design of next-generation materials, including mixed-metal, mixed-facet, and support-structured materials. By combining the fields of surface structure, material science, and application, meaningful progress can be made in the development of highly reactive NMO materials for a variety of applications. With this goal in mind, we believe there are many opportunities for scientific advancement and investigation that will help fill knowledge gaps going forward.

First, use of computational techniques, such as density functional theory (DFT) and molecular mechanics, to probe surface complexation, restructuring, adsorbate/adsorbate interactions, and adsorbate/solvent interactions will greatly enable a fundamental understanding of the thermodynamics and kinetics. These studies should be coupled with detailed electronic and atomic structure analyses to extract the fundamental interactions underpinning observable macroscopic interactions such as energies of surface complexation on NMO facets, redox chemistry, stability of surface structure, and electron exchange. Such studies have already greatly expanded our understanding of surface/adsorbate interactions and lead to new material designs with improved performance. This has been widely employed in metallic systems for choosing the most active facets and, more recently, metal oxides.[263,264]

However, current implementations of DFT limit what can be studied. Particularly, the poor scaling limits the length and time scales that are accessible and the accuracy of the current exchange–correlation functionals, which can lead to incorrect energy calculations. Most available methods scale with the cube of the number of electrons with a large pre-exponential factor,[265] which generally limits the system size to several hundred atoms and 1 or 2 ps. This problem can be partially alleviated by tools such as massively parallel computing systems, graphical processing units (GPU), linear scaling DFT, mixed molecular mechanics and quantum mechanics, and machine learning. Similarly, the porting of implicit solvent methods[266] from molecular quantum calculation codes into periodic boundary condition codes has decreased the cost of including solvents at solid interfaces, but the use of these tools is still quite restricted and expensive. These tools should be further developed to increase the system size that can be simulated to account for the complex and realistic surface environments. As new routes to rapid and accurate atomistic simulation are developed, it is important to include dynamic behavior into these studies.

Another key limitation is the accurate calculation of exchange and correlation energies. Most DFT calculations today rely on generalized gradient approximation (GGA) to calculate the exchange energy, *e.g.*, PBE,[267] which tends to overly delocalize electron density. Additionally, the electrons occupying the d-orbitals in most of the metal oxides described in this work are highly correlated, which is not accurately described. These effects can lead to large and unpredictable effects when calculating energies and oxidation states of the materials. Hybrid functionals, such as HSE06,[268] overcome some of the GGA limitations and tend to produce more accurate results, but they are computationally expensive. Despite the cost, they should be used in more works to benchmark the GGA results at a

minimum. Correlation effects are a more difficult problem to solve. The use of a Hubbard correction,[269] *i.e.* DFT+U, can eliminate unphysical partial occupation of d-orbitals and bring calculated energies in line with experience. However, a correct U penalty must be chosen, and the selection of the U parameter can be difficult when modeling multiple quantities simultaneously is desired. Just as reasonable empirical understandings inform computational calculations, so too should these calculations advise experimentalists on the material structure and composition to show the most promise in each of these environmental applications. The effective integration of these fields will require collaboration among computational chemists, material scientists, and engineers.

Second, recent instrumentation developments enabling robust characterization of surface structures and complexes should be applied to NMO facets to fully ascertain their structural and electronic behavior. Understanding surface structures, and particularly their transformation under a variety of environments, will be essential to ascribing facet-dependent behavior to different NMOs.[270] For example, synchrotron-based X-ray absorption fine structure (XAFS) and advanced techniques such as time-resolved XAFS, *operando* XAFS, and total reflection XAFS have been effective in investigating the local atomic structure of NMO facets and complexes, though definitive assignments of binding structures are often difficult, especially when the surface structure is not precisely known.[1,30,233,271,272] Crystal truncation rod (CTR) X-ray diffraction can distinguish similar binding structures on the same surface, though this technique utilizes cut and polished single-crystal samples, which may not be wholly representative of *in situ* sorption behavior of NMOs.[73,74] Raman spectroscopy is also a versatile technique successful at elucidating the defect chemistry of metal oxides, with *in situ* Raman spectroscopy probing these defects under varying environmental conditions.[30,273,274] Additionally, probe-molecule-assisted nuclear magnetic resonance (NMR) and *in situ* diffuse reflectance infrared Fourier transform spectroscopy (DRIFTS) have demonstrated their ability to discern surface structures and features of various facets.[275,276] *In situ* environmental (high-resolution) transmission electron microscopy (ETEM) and *in situ* liquid cell TEM can also be used to monitor the transformation and aggregation of metal oxide structures under realistic environmental conditions.[277–279] These techniques must be used in combination, as well as with computational approaches, in order to derive a complete picture of surface structure and complexation geometries. This will enable the elucidation of the underlying chemical structures and binding mechanisms before design for and implementation in catalytic, gas sensing, or sorptive applications. Relatedly, studies in application-relevant environments (*e.g.*, aqueous solutions, high temperatures, reducing conditions) will ensure that structural information used to elucidate performance is conducted in the same conditions.

Lastly, perhaps greater opportunities exist beyond facet reactivity in the development of facet *selectivity.*[248] Though some studies have reported differences in reactivity on different facets, fewer still have comprehensively explored the ability of different facets to promote selective behavior. In fact a more “reactive” facet may not necessarily be optimal for selectivity if molecules are bound indeterminately and/or too strongly.

Product selectivity in heterogeneous catalysis is highly desirable so as to maximize production efficiency while simultaneously minimizing waste production of unintended

byproducts and cost. However, true mechanistic understandings of catalytic selectivity cannot be evaluated solely by quantification of desired product but should instead be informed by each step of the catalytic reaction pathway. Recent work has shown the potential to realize product selectivity by strategic analysis of reactant, intermediate, *and* product binding strengths on different facets.[280] NMOs exposing facets that, due to their atomic structure, promote reaction pathways such that reactants and intermediates are both efficiently adsorbed and desorbed to form the desired product can be deliberately designed for intended applications. “Efficient” adsorption and desorption, however, must be understood in the context of binding energies and mechanistically modeled by computational calculations, rather than solely by empirical evidence.

Similarly, semiconductor gas sensors are known to be highly impeded in their sensing ability in the presence of many different gases, including water,[214] and would thus also benefit from improvements in selectivity. Since sensing abilities are highly dictated by electron transfer between gases and sensor surfaces, exploitation of differences in Fermi levels, metal electronegativity, and electric field polarization on different facets may make it possible to develop sensors sensitive to different classes of gases based on their reaction pathway and redox capabilities.[281,282] However, again, these facet-dependent differences in sensing selectivity must be grounded in a fundamental understanding of the structural and electronic characteristics of the sensing material as revealed by thorough spectrometric, computational, and surface-structure techniques.

Finally, in the sorption of contaminants, either for direct removal or photocatalyzed degradation, designing NMOs to target contaminants over competing species will ensure that the sorbent does not rapidly saturate.[248] In the past, quantum methods have been utilized to explain experimentally observed selective behavior, but advancements in computational capabilities have made possible the predictive ability of these methods. Screening for selective behavior by modeling the complexation geometries and binding energies of contaminants/competitors and NMO facets will allow for the informed design of promising selective materials for further experimental evaluation.[248] The power of computational and experimental developments in NMO facet selectivity will be enhanced if these techniques are used in conversation with one another, rather than used simply to explain one another.

In all, integrating computational modeling, empirical surface structure analysis, and experimental evaluation of catalytic, gas sensing, and sorptive performance will serve to strengthen our comprehension of NMO structure–property–function relationships, thus enabling the realization of NMOs’ full potential in these and other applications. Leveraging this robust understanding in the context of facet engineering will enhance functionality and inform advanced design of NMO materials for wide implementation. The scientific community can consequently begin a fundamental shift away from the “cook and look” methodology of empirically evaluating materials and toward a more comprehensive procedure in intentionally designing and developing our next-generation technologies from first principles.

Supplementary Material

Refer to Web version on PubMed Central for supplementary material.

ACKNOWLEDGMENTS

This work was supported by the National Science Foundation Nanosystems Engineering Research Center for Nanotechnology-Enabled Water Treatment (NEWT; Grant ERC-1449500) and the National Institute of Environmental Health Sciences of the National Institutes of Health Superfund Research Center Metals and Metals Mixtures: Cognitive Aging, Remediation, and Exposure Sources (MEMCARE; Grant P42ES030990). We thank Dr. Xiaopeng Huang and Dr. Hailiang Wang for their helpful correspondences during the writing of this work.

REFERENCES

(1). Huang X; Hou X; Zhang X; Rosso KM; Zhang L Facet-Dependent Contaminant Removal Properties of Hematite Nanocrystals and Their Environmental Implications. Environ. Sci.: Nano 2018, 5, 1790–1806.

(2). Pal J; Pal T Faceted Metal and Metal Oxide Nanoparticles: Design, Fabrication and Catalysis. Nanoscale 2015, 7, 14159–14190. [PubMed: 26255749]

(3). Gao X; Zhang T An Overview: Facet-Dependent Metal Oxide Semiconductor Gas Sensors. Sens. Actuators, B 2018, 277, 604–633.

(4). Cortés Corberán V; Rives V; Stathopoulos V Recent Applications of Nanometal Oxide Catalysts in Oxidation Reactions. Advanced Nanomaterials for Catalysis and Energy, 1st ed.; Elsevier: Cambridge, MA, USA, 2018; Vol. 1, pp 227–293, DOI: 10.1016/B978-0-12-814807-5.00007-3.

(5). Esswein AJ; McMurdo MJ; Ross PN; Bell AT; Tilley TD Size-Dependent Activity of Co3O4 Nanoparticle Anodes for Alkaline Water Electrolysis. J. Phys. Chem. C 2009, 113, 15068–15072.

(6). Zhou K; Li Y Catalysis Based on Nanocrystals with Well-Defined Facets. Angew. Chem., Int. Ed 2012, 51, 602–613.

(7). Hu L; Peng Q; Li Y Selective Synthesis of Co3O4 Nanocrystal with Different Shape and Crystal. J. Am. Chem. Soc 2008, 130, 16136–16137. [PubMed: 18998643]

(8). Ong WJ; Tan LL; Chai SP; Yong ST; Mohamed A R Facet-Dependent Photocatalytic Properties of TiO2-Based Composites for Energy Conversion and Environmental Remediation. ChemSusChem 2014, 7, 690–719. [PubMed: 24532412]

(9). Li Y; Shen W Morphology-Dependent Nanocatalysts: Rod-Shaped Oxides. Chem. Soc. Rev 2014, 43, 1543–1574. [PubMed: 24356335]

(10). Hristovski KD; Markovski J Engineering Metal (Hydr)Oxide Sorbents for Removal of Arsenate and Similar Weak-Acid Oxyanion Contaminants: A Critical Review with Emphasis on Factors Governing Sorption Processes. Sci. Total Environ 2017, 598, 258–271. [PubMed: 28445823]

(11). Trovarelli A; Llorca J Ceria Catalysts at Nanoscale: How Do Crystal Shapes Shape Catalysis? ACS Catal. 2017, 7, 4716–4735.

(12). Zhou K; Wang X; Sun X; Peng Q; Li Y Enhanced Catalytic Activity of Ceria Nanorods from Well-Defined Reactive Crystal Planes. J. Catal 2005, 229, 206–212.

(13). Liu G; Yang HG; Pan J; Yang YQ; Lu GQM; Cheng HM Titanium Dioxide Crystals with Tailored Facets. Chem. Rev 2014, 114, 9559–9612. [PubMed: 24851995]

(14). Xu H; Ouyang S; Liu L; Reunchan P; Umezawa N; Ye J Recent Advances in TiO2-Based Photocatalysis. J. Mater. Chem. A 2014, 2, 12642–12661.

(15). Zhuang L; Ge L; Yang Y; Li M; Jia Y; Yao X; Zhu Z Ultrathin Iron-Cobalt Oxide Nanosheets with Abundant Oxygen Vacancies for the Oxygen Evolution Reaction. Adv. Mater 2017, 29, 1606793.

(16). Gu XK; Carneiro JSA; Samira S; Das A; Ariyasingha NM; Nikolla E Efficient Oxygen Electrocatalysis by Nanostructured Mixed-Metal Oxides. J. Am. Chem. Soc 2018, 140, 8128–8137. [PubMed: 29847727]

(17). Li L; Feng X; Nie Y; Chen S; Shi F; Xiong K; Ding W; Qi X; Hu J; Wei Z; Wan L-J; Xia M Insight into the Effect of Oxygen Vacancy Concentration on the Catalytic Performance of MnO2. ACS Catal. 2015, 5, 4825–4832.

(18). Wu Z; Li M; Howe J; Meyer HM; Overbury SH Probing Defect Sites on CeO2 Nanocrystals with Well-Defined Surface Planes by Raman Spectroscopy and O2 Adsorption. Langmuir 2010, 26, 16595–16606. [PubMed: 20617854]

(19). Ji Y; Luo Y New Mechanism for Photocatalytic Reduction of CO2 on the Anatase TiO2(101) Surface: The Essential Role of Oxygen Vacancy. J. Am. Chem. Soc 2016, 138, 15896–15902. [PubMed: 27960337]

(20). Zhang N; Tsang EP; Chen J; Fang Z; Zhao D Critical Role of Oxygen Vacancies in Heterogeneous Fenton Oxidation over Ceria-Based Catalysts. J. Colloid Interface Sci 2020, 558, 163–172. [PubMed: 31586736]

(21). Muhich CL; Zhou Y; Holder AM; Weimer AW; Musgrave CB Effect of Surface Deposited Pt on the Photoactivity of TiO2. J. Phys. Chem. C 2012, 116, 10138–10149.

(22). Muhich CL; Westcott JY; Fuerst T; Weimer AW; Musgrave CB Increasing the Photocatalytic Activity of Anatase TiO2 through B, C, and N Doping. J. Phys. Chem. C 2014, 118, 27415–27427.

(23). Mason SE; Iceman CR; Tanwar KS; Trainor TP; Chaka AM Pb(II) Adsorption on Isostructural Hydrated Alumina and Hematite (0001) Surfaces: A DFT Study. J. Phys. Chem. C 2009, 113, 2159–2170.

(24). Parkinson GS Iron Oxide Surfaces. Surf. Sci. Rep 2016, 71, 272–365.

(25). Gautier-Soyer M; Pollak M; Henriot M; Guittet MJ The (1 × 2) Reconstruction of the α-Fe2O3 (1012) Surface. Surf. Sci 1996, 352–354, 112–116.

(26). Goniakowski J; Finocchi F; Noguera C Polarity of Oxide Surfaces and Nanostructures. Rep. Prog. Phys 2008, 71, 016501.

(27). Tasker PW The Stability of Ionic Crystal Surfaces. J. Phys. C: Solid State Phys 1979, 12, 4977–4984.

(28). Mason SE; Iceman CR; Trainor TP; Chaka AM Density Functional Theory Study of Clean, Hydrated, and Defective Alumina (1102) Surfaces. Phys. Rev. B: Condens. Matter Mater. Phys 2010, 81, 125423.

(29). Trovarelli A Catalytic Properties of Ceria and CeO2-Containing Materials. Catal. Rev.: Sci. Eng 1996, 38, 439–520.

(30). Schmitt R; Nenning A; Kraynis O; Korobko R; Frenkel AI; Lubomirsky I; Haile SM; Rupp JLM A Review of Defect Structure and Chemistry in Ceria and Its Solid Solutions. Chem. Soc. Rev 2020, 49, 554–592. [PubMed: 31872840]

(31). Zang C; Zhang X; Hu S; Chen F The Role of Exposed Facets in the Fenton-Like Reactivity of CeO2 Nanocrystal to the Orange II. Appl. Catal., B 2017, 216, 106–113.

(32). Chen X; Yang H; Au C; Tian S; Xiong Y; Chang Y Efficiency and Mechanism of Pollutant Degradation and Bromate Inhibition by Faceted CeO2 Catalyzed Ozonation: Experimental and Theoretical Study. Chem. Eng. J 2020, 390, 124480.

(33). Li P; Chen X; Li Y; Schwank JW A Review on Oxygen Storage Capacity of CeO2-Based Materials: Influence Factors, Measurement Techniques, and Applications in Reactions Related to Catalytic Automotive Emissions Control. Catal. Today 2019, 327, 90–115.

(34). Campbell CT; Peden CHF Oxygen Vacancies and Catalysis on Ceria Surfaces. Science 2005, 309, 713–714. [PubMed: 16051777]

(35). Mullins D R The Surface Chemistry of Cerium Oxide. Surf. Sci. Rep 2015, 70, 42–85.

(36). Naghavi SS; Emery AA; Hansen HA; Zhou F; Ozolins V; Wolverton C Giant Onsite Electronic Entropy Enhances the Performance of Ceria for Water Splitting. Nat. Commun 2017, 8, 285. [PubMed: 28819153]

(37). Chueh WC; Falter C; Abbott M; Scipio D; Furler P; Haile SM; Steinfeld A High-Flux Solar-Driven Thermochemical Dissociation of CO_2 and H_2O Using Nonstoichiometric Ceria. Science 2010, 330, 1797–1801. [PubMed: 21205663]

(38). Grieshammer S; Zacherle T; Martin M Entropies of Defect Formation in Ceria from First Principles. Phys. Chem. Chem. Phys 2013, 15, 15935–15942. [PubMed: 23955537]

(39). Majumder D; Chakraborty I; Mandal K; Roy S Facet-Dependent Photodegradation of Methylene Blue Using Pristine CeO2 Nanostructures. ACS Omega 2019, 4, 4243–4251. [PubMed: 31459631]

(40). Conesa J Computer Modeling of Surfaces and Defects on Cerium Dioxide. Surf. Sci 1995, 339, 337–352.

(41). Wu Z; Li M; Overbury SH On the Structure Dependence of CO Oxidation over CeO 2 Nanocrystals with Well-Defined Surface Planes. J. Catal 2012, 285, 61–73.

(42). Nolan M; Fearon JE; Watson GW Oxygen Vacancy Formation and Migration in Ceria. Solid State Ionics 2006, 177, 3069–3074.

(43). Jiang D; Wang W; Zhang L; Zheng Y; Wang Z Insights into the Surface-Defect Dependence of Photoreactivity over CeO2 Nanocrystals with Well-Defined Crystal Facets. ACS Catal. 2015, 5, 4851–4858.

(44). Polo-Garzon F; Bao Z; Zhang X; Huang W; Wu Z Surface Reconstructions of Metal Oxides and the Consequences on Catalytic Chemistry. ACS Catal. 2019, 9, 5692–5707.

(45). Ganduglia-Pirovano MV; Hofmann A; Sauer J Oxygen Vacancies in Transition Metal and Rare Earth Oxides: Current State of Understanding and Remaining Challenges. Surf. Sci. Rep 2007, 62, 219–270.

(46). Wu Z; Mann AKP; Li M; Overbury SH Spectroscopic Investigation of Surface Dependent Acid Base Property of Ceria Nanoshapes. J. Phys. Chem. C 2015, 119, 7340–7350.

(47). Metiu H; Chrétien S; Hu Z; Li B; Sun X Chemistry of Lewis Acid-Base Pairs on Oxide Surfaces. J. Phys. Chem. C 2012, 116, 10439–10450.

(48). Wang S; Zhao L; Wang W; Zhao Y; Zhang G; Ma X; Gong J Morphology Control of Ceria Nanocrystals for Catalytic Conversion of CO2 with Methanol. Nanoscale 2013, 5, 5582–5588. [PubMed: 23680853]

(49). Sun H; Ang HM; Tadé MO; Wang S Co3O4 Nanocrystals with Predominantly Exposed Facets: Synthesis, Environmental and Energy Applications. J. Mater. Chem. A 2013, 1, 14427–14442.

(50). Liu Q; Chen Z; Yan Z; Wang Y; Wang E; Wang SS; Wang SS; Sun G Crystal-Plane-Dependent Activity of Spinel Co3O4 Towards Water Splitting and the Oxygen Reduction Reaction. ChemElectroChem 2018, 5, 1080–1086.

(51). Royer S; Duprez D Catalytic Oxidation of Carbon Monoxide over Transition Metal Oxides. ChemCatChem 2011, 3, 24–65.

(52). Xu X-L; Chen Z-H; Li Y; Chen W-K; Li J-Q Bulk and Surface Properties of Spinel Co3O4 by Density Functional Calculations. Surf. Sci 2009, 603, 653–658.

(53). Wang HF; Kavanagh R; Guo YYL; Guo YYL; Lu G; Hu P Origin of Extraordinarily High Catalytic Activity of Co3O 4 and Its Morphological Chemistry for CO Oxidation at Low Temperature. J. Catal 2012, 296, 110–119.

(54). Chen J; Selloni A Water Adsorption and Oxidation at the Co3O4 (110) Surface. J. Phys. Chem. Lett 2012, 3, 2808–2814.

(55). Yan G; Sautet P Surface Structure of Co3O4 (111) under Reactive Gas-Phase Environments. ACS Catal. 2019, 9, 6380–6392.

(56). Chen Z; Kronawitter CX; Koel BE Facet-Dependent Activity and Stability of Co3O4 Nanocrystals towards the Oxygen Evolution Reaction. Phys. Chem. Chem. Phys 2015, 17, 29387–29393. [PubMed: 26473390]

(57). Zasada F; Piskorz W; Cristol S; Paul J-F; Kotarba A; Sojka Z Periodic Density Functional Theory and Atomistic Thermodynamic Studies of Cobalt Spinel Nanocrystals in Wet Environment: Molecular Interpretation of Water Adsorption Equilibria. J. Phys. Chem. C 2010, 114, 22245–22253.

(58). Sun S; Zhang XX; Yang Q; Liang S; Zhang XX; Yang Z Cuprous Oxide (Cu2O) Crystals with Tailored Architectures: A Comprehensive Review on Synthesis, Fundamental Properties, Functional Modifications and Applications. Prog. Mater. Sci 2018, 96, 111–173.

(59). Shang Y; Guo L Facet-Controlled Synthetic Strategy of Cu2O-Based Crystals for Catalysis and Sensing. Adv. Sci 2015, 2, 1500140.

(60). Nilius N; Fedderwitz H; Groß B; Noguera C; Goniakowski J Incorrect DFT-GGA Predictions of the Stability of Non-Stoichiometric/Polar Dielectric Surfaces: The Case of Cu2O(111). Phys. Chem. Chem. Phys 2016, 18, 6729–6733. [PubMed: 26876056]

(61). Soldemo M; Stenlid JH; Besharat Z; Ghadami Yazdi M; Önsten A; Leygraf C; Göthelid M; Brinck T; Weissenrieder J The Surface Structure of Cu2O(100). J. Phys. Chem. C 2016, 120, 4373–4381.

(62). Cornell RM; Schwertmann U The Iron Oxides: Structure, Properties, Reactions, Occurences, and Uses, 2nd ed.; Wiley-VCH: Weinheim, Germany, 2003; DOI: 10.1002/3527602097.

(63). Tanwar KS; Catalano JG; Petitto SC; Ghose SK; Eng PJ; Trainor TP Hydrated α-Fe2O3(1102) Surface Structure: Role of Surface Preparation. Surf. Sci 2007, 601, L59–L64.

(64). Catalano JG Weak Interfacial Water Ordering on Isostructural Hematite and Corundum (001) Surfaces. Geochim. Cosmochim. Acta 2011, 75, 2062–2071.

(65). Trainor TP; Chaka AM; Eng PJ; Newville M; Waychunas GA; Catalano JG; Brown GE Structure and Reactivity of the Hydrated Hematite (0001) Surface. Surf. Sci 2004, 573, 204–224.

(66). Catalano JG; Fenter P; Park C Water Ordering and Surface Relaxations at the Hematite (1 1 0)-Water Interface. Geochim. Cosmochim. Acta 2009, 73, 2242–2251.

(67). Huang X; Hou X; Song F; Zhao J; Zhang L Facet-Dependent Cr(VI) Adsorption of Hematite Nanocrystals. Environ. Sci. Technol 2016, 50, 1964–1972. [PubMed: 26815307]

(68). Tanwar KS; Lo CS; Eng PJ; Catalano JG; Walko DA; Brown GE; Waychunas GA; Chaka AM; Trainor TP Surface Diffraction Study of the Hydrated Hematite (1102) Surface. Surf. Sci 2007, 601, 460–474.

(69). Catalano JG; Zhang Z; Park C; Fenter P; Bedzyk MJ Bridging Arsenate Surface Complexes on the Hematite (0 1 2) Surface. Geochim. Cosmochim. Acta 2007, 71, 1883–1897.

(70). McBriarty ME; Stubbs JE; Eng PJ; Rosso KM Reductive Dissolution Mechanisms at the Hematite-Electrolyte Interface Probed by *in Situ* X-Ray Scattering. J. Phys. Chem. C 2019, 123, 8077–8085.

(71). Catalano JG; Park C; Fenter P; Zhang Z Simultaneous Inner- and Outer-Sphere Arsenate Adsorption on Corundum and Hematite. Geochim. Cosmochim. Acta 2008, 72, 1986–2004.

(72). Huang X; Chen Y; Walter E; Zong M; Wang Y; Zhang X; Qafoku O; Wang Z; Rosso KM Facet-Specific Photocatalytic Degradation of Organics by Heterogeneous Fenton Chemistry on Hematite Nanoparticles. Environ. Sci. Technol 2019, 53, 10197–10207. [PubMed: 31397154]

(73). Qiu C; Majs F; Eng PJ; Stubbs JE; Douglas TA; Schmidt M; Trainor TP *In Situ* Structural Study of the Surface Complexation of Lead(II) on the Chemically Mechanically Polished Hematite (11-02) Surface. J. Colloid Interface Sci 2018, 524, 65–75. [PubMed: 29631220]

(74). Qiu C; Chen W; Schmidt M; Majs F; Douglas TA; Trainor TP Selective Adsorption of Pb(II) on an Annealed Hematite (1102) Surface: Evidence from Crystal Truncation Rod X-Ray Diffraction and Density Functional Theory. Environ. Sci. Technol 2020, 54, 6651–6660.

(75). McBriarty ME; Von Rudorff GF; Stubbs JE; Eng PJ; Blumberger J; Rosso KM Dynamic Stabilization of Metal Oxide-Water Interfaces. J. Am. Chem. Soc 2017, 139, 2581–2584. [PubMed: 28173705]

(76). Noerpel MR; Lee SS; Lenhart JJ X-Ray Analyses of Lead Adsorption on the (001), (110), and (012) Hematite Surfaces. Environ. Sci. Technol 2016, 50, 12283–12291. [PubMed: 27767293]

(77). Yamamoto S; Kendelewicz T; Newberg JT; Ketteler G; Starr DE; Mysak ER; Andersson KJ; Ogasawara H; Bluhm H; Salmeron M; Brown GE; Nilsson A Water Adsorption on α-Fe2O3 (0001) at near Ambient Conditions. J. Phys. Chem. C 2010, 114, 2256–2266.

(78). Wang XG; Weiss W; Shaikhutdinov Sh. K.; Ritter M; Petersen M; Wagner F; Schloegl R; Scheffler M The Hematite α-Fe_2O_3) (0001) Surface: Evidence for Domains of Distinct Chemistry. Phys. Rev. Lett 1998, 81, 1038–1041.

(79). Guo H; Barnard AS Environmentally Dependent Stability of Low-Index Hematite Surfaces. J. Colloid Interface Sci 2012, 386, 315–324. [PubMed: 22918051]

(80). Rohrbach A; Hafner J; Kresse G *Ab Initio* Study of the (0001) Surfaces of Hematite and Chromia: Influence of Strong Electronic Correlations. Phys. Rev. B: Condens. Matter Mater. Phys 2004, 70, 1–17.

(81). Cao S; Zhang X; Huang X; Wan S; An X; Jia F; Zhang L Insights into the Facet-Dependent Adsorption of Phenylarsonic Acid on Hematite Nanocrystals. Environ. Sci.: Nano 2019, 6, 3280–3291.

(82). Mackrodt WC Atomistic Simulation of Oxide Surfaces. Phys. Chem. Miner 1988, 15, 228–237.

(83). Guo H; Barnard AS Thermodynamic Modelling of Nanomorphologies of Hematite and Goethite. J. Mater. Chem 2011, 21, 11566–11577.

(84). Batzill M; Katsiev K; Burst JM; Diebold U; Chaka AM; Delley B Gas-Phase-Dependent Properties of SnO2 (110), (100), and (101) Single-Crystal Surfaces: Structure, Composition, and Electronic Properties. Phys. Rev. B: Condens. Matter Mater. Phys 2005, 72, 1–20.

(85). Wang X; Han X; Xie S; Kuang Q; Jiang Y; Zhang S; Mu X; Chen G; Xie Z; Zheng L Controlled Synthesis and Enhanced Catalytic and Gas-Sensing Properties of Tin Dioxide Nanoparticles with Exposed High-Energy Facets. Chem. - Eur. J 2012, 18, 2283–2289. [PubMed: 22266637]

(86). Han X; Jin M; Xie S; Kuang Q; Jiang Z; Jiang Y; Xie Z; Zheng L Synthesis of Tin Dioxide Octahedral Nanoparticles with Exposed High-Energy {221} Facets and Enhanced Gas-Sensing Properties. Angew. Chem., Int. Ed 2009, 48, 9180–9183.

(87). Batzill M; Diebold U The Surface and Materials Science of Tin Oxide. Prog. Surf. Sci 2005, 79, 47–154.

(88). Lazzeri M; Vittadini A; Selloni A Structure and Energetics of Stoichiometric TiO2 Anatase Surfaces. Phys. Rev. B: Condens. Matter Mater. Phys 2001, 63, 1554091–1554099.

(89). Luttrell T; Halpegamage S; Tao J; Kramer A; Sutter E; Batzill M Why Is Anatase a Better Photocatalyst than Rutile? - Model Studies on Epitaxial TiO2 Films. Sci. Rep 2015, 4, 1–8.

(90). Diebold U; Ruzycki N; Herman GS; Selloni A One Step towards Bridging the Materials Gap: Surface Studies of TiO2 Anatase. Catal. Today 2003, 85, 93–100.

(91). Pan J; Liu G; Lu GQ; Cheng HM On the True Photoreactivity Order of {001}, {010}, and {101} Facets of Anatase TiO2 Crystals. Angew. Chem., Int. Ed 2011, 50, 2133–2137.

(92). Maisano M; Dozzi MV; Selli E Journal of Photochemistry and Photobiology C : Photochemistry Reviews Searching for Facet-Dependent Photoactivity of Shape-Controlled Anatase TiO 2. J. Photochem. Photobiol, C 2016, 28, 29–43.

(93). Katal R; Masudy-Panah S; Tanhaei M; Farahani MHDA; Jiangyong H A Review on the Synthesis of the Various Types of Anatase TiO_2 Facets and Their Applications for Photocatalysis. Chem. Eng. J 2020, 384, 123384.

(94). Wang ZL Zinc Oxide Nanostructures: Growth, Properties and Applications. J. Phys.: Condens. Matter 2004, 16, R829–R858.

(95). Meyer B; Marx D Density-Functional Study of the Structure and Stability of ZnO Surfaces. Phys. Rev. B: Condens. Matter Mater. Phys 2003, 67, 1–11.

(96). Mora-Fonz D; Lazauskas T; Farrow MR; Catlow CRA; Woodley SM; Sokol AA Why Are Polar Surfaces of ZnO Stable? Chem. Mater 2017, 29, 5306–5320.

(97). Wöll C The Chemistry and Physics of Zinc Oxide Surfaces. Prog. Surf. Sci 2007, 82, 55–120.

(98). Guan M; Xiao C; Zhang J; Fan S; An R; Cheng Q; Xie J; Zhou M; Ye B; Xie Y Vacancy Associates Promoting Solar-Driven Photocatalytic Activity of Ultrathin Bismuth Oxychloride Nanosheets. J. Am. Chem. Soc 2013, 135, 10411–10417. [PubMed: 23782301]

(99). Huang WC; Lyu LM; Yang YC; Huang MH Synthesis of Cu 2O Nanocrystals from Cubic to Rhombic Dodecahedral Structures and Their Comparative Photocatalytic Activity. J. Am. Chem. Soc 2012, 134, 1261–1267. [PubMed: 22257266]

(100). Zhang L; Gonçalves AAS; Jaroniec M Identification of Preferentially Exposed Crystal Facets by X-Ray Diffraction. RSC Adv. 2020, 10, 5585–5589. [PubMed: 35497459]

(101). Zhou W; Greer HF What Can. Electron Microscopy Tell Us beyond Crystal Structures? Eur. J. Inorg. Chem 2016, 2016, 941–950.

(102). Fang WQ; Gong X-Q; Yang HG On the Unusual Properties of Anatase TiO2 Exposed by Highly Reactive Facets. J. Phys. Chem. Lett 2011, 2, 725–734.

(103). Afzal S; Quan X; Lu S Catalytic Performance and an Insight into the Mechanism of CeO2 Nanocrystals with Different Exposed Facets in Catalytic Ozonation of P-Nitrophenol. Appl. Catal., B 2019, 248, 526–537.

(104). Fisher TJ; Zhou Y; Wu TS; Wang M; Soo YL; Cheung CL Structure-Activity Relationship of Nanostructured Ceria for the Catalytic Generation of Hydroxyl Radicals. Nanoscale 2019, 11, 4552–4561. [PubMed: 30806412]

(105). Mu J; Zhang L; Zhao M; Wang Y Catalase Mimic Property of Co3O4 Nanomaterials with Different Morphology and Its Application as a Calcium Sensor. ACS Appl. Mater. Interfaces 2014, 6, 7090–7098. [PubMed: 24796855]

(106). Mu J; Zhang L; Zhao G; Wang Y The Crystal Plane Effect on the Peroxidase-Like Catalytic Properties of Co3O4 Nanomaterials. Phys. Chem. Chem. Phys 2014, 16, 15709–15716. [PubMed: 24960303]

(107). Liang Y; Shang L; Bian T; Zhou C; Zhang D; Yu H; Xu H; Shi Z; Zhang T; Wu LZ; Tung CH Shape-Controlled Synthesis of Polyhedral 50-Facet Cu 2O Microcrystals with High-Index Facets. CrystEngComm 2012, 14, 4431–4436.

(108). Zhang DF; Zhang H; Guo L; Zheng K; Han XD; Zhang Z Delicate Control of Crystallographic Facet-Oriented Cu2O Nanocrystals and the Correlated Adsorption Ability. J. Mater. Chem 2009, 19, 5220–5225.

(109). Ho WCJ; Tay Q; Qi H; Huang Z; Li J; Chen Z Photocatalytic and Adsorption Performances of Faceted Cuprous Oxide (Cu2O) Particles for the Removal of Methyl Orange (MO) from Aqueous Media. Molecules 2017, 22, 677.

(110). Ho JY; Huang MH Synthesis of Submicrometer-Sized Cu2O Crystals with Morphological Evolution from Cubic to Hexapod Structures and Their Comparative Photocatalytic Activity. J. Phys. Chem. C 2009, 113, 14159–14164.

(111). Xu H; Wang W; Zhu W Shape Evolution and Size-Controllable Synthesis of Cu2O Octahedra and Their Morphology-Dependent Photocatalytic Properties. J. Phys. Chem. B 2006, 110, 13829–13834. [PubMed: 16836330]

(112). Kuo CH; Huang MH Facile Synthesis of Cu2O Nanocrystals with Systematic Shape Evolution from Cubic to Octahedral Structures. J. Phys. Chem. C 2008, 112, 18355–18360.

(113). Zhao Y; Pan F; Li H; Niu T; Xu G; Chen W Facile Synthesis of Uniform α-Fe2O3 Crystals and Their Facet-Dependent Catalytic Performance in the Photo-Fenton Reaction. J. Mater. Chem. A 2013, 1, 7242–7246.

(114). Zhou X; Lan J; Liu G; Deng K; Yang Y; Nie G; Yu J; Zhi L Facet-Mediated Photodegradation of Organic Dye over Hematite Architectures by Visible Light. Angew. Chem. Int. Ed 2012, 51, 178–182.

(115). Wu W; Hao R; Liu F; Su X; Hou Y Single-Crystalline α-Fe2O3 Nanostructures: Controlled Synthesis and High-Index Plane-Enhanced Photodegradation by Visible Light. J. Mater. Chem. A 2013, 1, 6888–6894.

(116). Huang X; Hou X; Zhao J; Zhang L Hematite Facet Confined Ferrous Ions as High Efficient Fenton Catalysts to Degrade Organic Contaminants by Lowering H2O2 Decomposition Energetic Span. Appl. Catal, B 2016, 181, 127–137.

(117). Wang X; Wang J; Cui Z; Wang S; Cao M Facet Effect of α-Fe2O3 Crystals on Photocatalytic Performance in the Photo-Fenton Reaction. RSC Adv. 2014, 4, 34387–34394.

(118). Chan JYT; Ang SY; Ye EY; Sullivan M; Zhang J; Lin M Heterogeneous Photo-Fenton Reaction on Hematite (α-Fe2O3) {104}, {113} and {001} Surface Facets. Phys. Chem. Chem. Phys 2015, 17, 25333–25341. [PubMed: 26355813]

(119). Huang X; Hou X; Jia F; Song F; Zhao J; Zhang L Ascorbate-Promoted Surface Iron Cycle for Efficient Heterogeneous Fenton Alachlor Degradation with Hematite Nanocrystals. ACS Appl. Mater. Interfaces 2017, 9, 8751–8758. [PubMed: 28240850]

(120). Patra AK; Kundu SK; Bhaumik A; Kim D Morphology Evolution of Single-Crystalline Hematite Nanocrystals: Magnetically Recoverable Nanocatalysts for Enhanced Facet-Driven Photoredox Activity. Nanoscale 2016, 8, 365–377. [PubMed: 26616162]

(121). Kislov N; Lahiri J; Verma H; Goswami DY; Stefanakos E; Batzill M Photocatalytic Degradation of Methyl Orange over Single Crystalline ZnO: Orientation Dependence of Photoactivity and Photostability of ZnO. Langmuir 2009, 25, 3310–3315. [PubMed: 19437731]

(122). Mai HX; Sun LD; Zhang YW; Si R; Feng W; Zhang HP; Liu HC; Yan CH Shape-Selective Synthesis and Oxygen Storage Behavior of Ceria Nanopolyhedra, Nanorods, and Nanocubes. J. Phys. Chem. B 2005, 109, 24380–24385. [PubMed: 16375438]

(123). Piumetti M; Andana T; Bensaid S; Russo N; Fino D; Pirone R Study on the CO Oxidation over Ceria-Based Nanocatalysts. Nanoscale Res. Lett 2016, 11, 165. [PubMed: 27009532]

(124). Teng Y; Kusano Y; Azuma M; Haruta M; Shimakawa Y Morphology Effects of Co3O4 Nanocrystals Catalyzing CO Oxidation in a Dry Reactant Gas Stream. Catal. Sci. Technol 2011, 1, 920–922.

(125). Hu L; Sun K; Peng Q; Xu B; Li Y Surface Active Sites on Co3O4 Nanobelt and Nanocube Model Catalysts for CO Oxidation. Nano Res. 2010, 3, 363–368.

(126). Chen Z; Wang SS; Liu W; Gao X; Gao D; Wang M; Wang SS Morphology-Dependent Performance of Co3O4 via Facile and Controllable Synthesis for Methane Combustion. Appl. Catal. A 2016, 525, 94–102.

(127). Ma CY; Mu Z; Li JJ; Jin YG; Cheng J; Lu GQ; Hao ZP; Qiao SZ Mesoporous Co3O4 and Au/Co3O4 Catalysts for Low-Temperature Oxidation of Trace Ethylene. J. Am. Chem. Soc 2010, 132, 2608–2613. [PubMed: 20141130]

(128). Zhou L; Cao S; Zhang L; Xiang G; Wang J; Zeng X; Chen J Facet Effect of Co3O4 Nanocatalysts on the Catalytic Decomposition of Ammonium Perchlorate. J. Hazard. Mater 2020, 392, 122358. [PubMed: 32109796]

(129). Leng M; Liu M; Zhang Y; Wang Z; Yu C; Yang X; Zhang H; Wang C Polyhedral 50-Facet Cu2O Microcrystals Partially Enclosed by {311} High-Index Planes: Synthesis and Enhanced Catalytic CO Oxidation Activity. J. Am. Chem. Soc 2010, 132, 17084–17087. [PubMed: 21073152]

(130). Hua Q; Cao T; Bao H; Jiang Z; Huang W Crystal-Plane-Controlled Surface Chemistry and Catalytic Performance of Surfactant-Free Cu2O Nanocrystals. ChemSusChem 2013, 6, 1966–1972. [PubMed: 24106201]

(131). Bao H; Zhang W; Hua Q; Jiang Z; Yang J; Huang W Crystal-Plane-Controlled Surface Restructuring and Catalytic Performance of Oxide Nanocrystals. Angew. Chem., Int. Ed 2011, 50, 12294–12298.

(132). Hua Q; Cao T; Gu XK; Lu J;Jiang Z; Pan X; Luo L; Li WX; Huang W Crystal-Plane-Controlled Selectivity of Cu2O Catalysts in Propylene Oxidation with Molecular Oxygen. Angew. Chem., Int. Ed 2014, 53, 4856–4861.

(133). Sun L; Zhan W; Li YA; Wang F; Zhang X; Han X Understanding the Facet-Dependent Catalytic Performance of Hematite Microcrystals in a CO Oxidation Reaction. Inorg. Chem. Front 2018, 5, 2332–2339.

(134). Ouyang J; Pei J; Kuang Q; Xie Z; Zheng L Supersaturation-Controlled Shape Evolution of α-Fe2O 3 Nanocrystals and Their Facet-Dependent Catalytic and Sensing Properties. ACS Appl. Mater. Interfaces 2014, 6, 12505–12514. [PubMed: 25003988]

(135). Liu X; Liu J; Chang Z; Sun X; Li Y Crystal Plane Effect of Fe2O3 with Various Morphologies on CO Catalytic Oxidation. Catal. Commun 2011, 12, 530–534.

(136). Zhou X; Liu Z; Wang Y; Ding Y Facet Effect of Co3O4 Nanocrystals on Visible-Light Driven Water Oxidation. Appl. Catal. B 2018, 237, 74–84.

(137). Liu L; Jiang Z; Fang L; Xu H; Zhang H; Gu X; Wang Y Probing the Crystal Plane Effect of Co_3O_4 for Enhanced Electrocatalytic Performance toward Efficient Overall Water Splitting. ACS Appl. Mater. Interfaces 2017, 9, 27736–27744. [PubMed: 28758720]

(138). Li W; Yang KR; Yao X; He Y; Dong Q; Brudvig GW; Batista VS; Wang D Facet-Dependent Kinetics and Energetics of Hematite for Solar Water Oxidation Reactions. ACS Appl. Mater. Interfaces 2019, 11, 5616–5622. [PubMed: 29792412]

(139). Wu H; Yang T; Du Y; Shen L; Ho GW Identification of Facet-Governing Reactivity in Hematite for Oxygen Evolution. Adv. Mater 2018, 30, 1804341.

(140). Takashima T; Hemmi S; Liu Q; Irie H Facet-Dependent Activity of Hematite Nanocrystals toward the Oxygen Evolution Reaction. Catal. Sci. Technol 2020, 10, 3748–3754.

(141). Zhao EW; Zheng H; Zhou R; Hagelin-Weaver HE; Bowers CR Shaped Ceria Nanocrystals Catalyze Efficient and Selective Para-Hydrogen-Enhanced Polarization. Angew. Chem. Int. Ed 2015, 54, 14270–14275.

(142). Vilé G; Colussi S; Krumeich F; Trovarelli A; Pérez-Ramírez J Opposite Face Sensitivity of CeO2 in Hydrogenation and Oxidation Catalysis. Angew. Chem. Int. Ed 2014, 53, 12069–12072.

(143). Zhao EW; Xin Y; Hagelin-Weaver HE; Bowers CR Semihydrogenation of Propyne over Cerium Oxide Nanorods, Nanocubes, and Nano-Octahedra: Facet-Dependent Parahydrogen-Induced Polarization. ChemCatChem 2016, 8, 2197–2201.

(144). Wang X; Ding L; Zhao Z; Xu W; Meng B; Qiu J Novel Hydrodesulfurization Nano-Catalysts Derived from Co3O 4 Nanocrystals with Different Shapes. Catal. Today 2011, 175, 509–514.

(145). Chanda K; Rej S; Huang MH Investigation of Facet Effects on the Catalytic Activity of Cu2O Nanocrystals for Efficient Regioselective Synthesis of 3,5-Disubstituted Isoxazoles. Nanoscale 2013, 5, 12494–12501. [PubMed: 24165690]

(146). Chanda K; Rej S; Huang MH Facet-Dependent Catalytic Activity of Cu2O Nanocrystals in the One-Pot Synthesis of 1,2,3-Triazoles by Multicomponent Click Reactions. Chem. - Eur. J 2013, 19, 16036–16043. [PubMed: 24127396]

(147). Xu Y; Wang H; Yu Y; Tian L; Zhao W; Zhang B Cu2O Nanocrystals: Surfactant-Free Room-Temperature Morphology-Modulated Synthesis and Shape-Dependent Heterogeneous Organic Catalytic Activities. J. Phys. Chem. C 2011, 115, 15288–15296.

(148). Lee KM; Lai CW; Ngai KS; Juan JC Recent Developments of Zinc Oxide Based Photocatalyst in Water Treatment Technology: A Review. Water Res. 2016, 88, 428–448. [PubMed: 26519627]

(149). Bokare AD; Choi W Review of Iron-Free Fenton-Like Systems for Activating H2O2 in Advanced Oxidation Processes. J. Hazard. Mater 2014, 275, 121–135. [PubMed: 24857896]

(150). Chen F; Shen X; Wang Y; Zhang J CeO 2/H 2O 2 System Catalytic Oxidation Mechanism Study via a Kinetics Investigation to the Degradation of Acid Orange 7. Appl. Catal., B 2012, 121–122, 223–229.

(151). Wu T; Liu G; Zhao J; Hidaka H; Serpone N Evidence for H2O2 Generation during the TiO2-Assisted Photodegradation of Dyes in Aqueous Dispersions under Visible Light Illumination. J. Phys. Chem. B 1999, 103, 4862–4867.

(152). Nidheesh PV; Gandhimathi R; Ramesh ST Degradation of Dyes from Aqueous Solution by Fenton Processes: A Review. Environ. Sci. Pollut. Res 2013, 20, 2099–2132.

(153). Wang Y; Hong CS Effect of Hydrogen Peroxide, Periodate and Persulfate on Photocatalysis of 2-Chlorobiphenyl in Aqueous TiO2 Suspensions. Water Res. 1999, 33, 2031–2036.

(154). Zhu Y; Zhu R; Xi Y; Zhu J; Zhu G; He H Strategies for Enhancing the Heterogeneous Fenton Catalytic Reactivity: A Review. Appl. Catal., B 2019, 255, 117739.

(155). Baran T; Wojtyla S; Minguzzi A; Rondinini S; Vertova A Achieving Efficient H2O2 Production by a Visible-Light Absorbing, Highly Stable Photosensitized TiO2. Appl. Catal., B 2019, 244, 303–312.

(156). Li H; Shang J; Yang Z; Shen W; Ai Z; Zhang L Oxygen Vacancy Associated Surface Fenton Chemistry: Surface Structure Dependent Hydroxyl Radicals Generation and Substrate Dependent Reactivity. Environ. Sci. Technol 2017, 51, 5685–5694. [PubMed: 28418239]

(157). Wu X-P; Gong X-Q Clustering of Oxygen Vacancies at CeO_2 (111): Critical Role of Hydroxyls. Phys. Rev. Lett 2016, 116, 86102.

(158). Yang HG; Liu G; Qiao SZ; Sun CH; Jin YG; Smith SC; Zou J; Cheng HM; Lu GQ Solvothermal Synthesis and Photoreactivity of Anatase TiO2 Nanosheets with Dominant {001} Facets. J. Am. Chem. Soc 2009, 131, 4078–4083. [PubMed: 19249825]

(159). Liu G; Yang HG; Wang X; Cheng L; Pan J; Lu GQM; Cheng H-M Visible Light Responsive Nitrogen Doped Anatase TiO2 Sheets with Dominant {001} Facets Derived from TiN. J. Am. Chem. Soc 2009, 131, 12868–12869. [PubMed: 19697930]

(160). Liu B; Huang Y; Wen Y; Du L; Zeng W; Shi Y; Zhang F; Zhu G; Xu X; Wang Y Highly Dispersive {001} Facets-Exposed Nanocrystalline TiO2 on High Quality Graphene as a High Performance Photocatalyst. J. Mater. Chem 2012, 22, 7484–7491.

(161). Liu M; Piao L; Lu W; Ju S; Zhao L; Zhou C; Li H; Wang W Flower-Like TiO2 Nanostructures with Exposed {001} Facets: Facile Synthesis and Enhanced Photocatalysis. Nanoscale 2010, 2, 1115–1117. [PubMed: 20644783]

(162). Xiang Q; Lv K; Yu J Pivotal Role of Fluorine in Enhanced Photocatalytic Activity of Anatase TiO2 Nanosheets with Dominant (001) Facets for the Photocatalytic Degradation of Acetone in Air. Appl. Catal., B 2010, 96, 557–564.

(163). Gordon TR; Cargnello M; Paik T; Mangolini F; Weber RT; Fornasiero P; Murray CB Nonaqueous Synthesis of TiO 2 Nanocrystals Using TiF 4 to Engineer Morphology, Oxygen Vacancy Concentration, and Photocatalytic Activity. J. Am. Chem. Soc 2012, 134, 6751–6761. [PubMed: 22444667]

(164). Zhang Y; Deng B; Zhang T; Gao D; Xu AW Shape Effects of Cu2O Polyhedral Microcrystals on Photocatalytic Activity. J. Phys. Chem. C 2010, 114, 5073–5079.

(165). Wang L; Deo S; Dooley K; Janik MJ; Rioux RM Influence of Metal Nuclearity and Physicochemical Properties of Ceria on the Oxidation of Carbon Monoxide. Chin. J. Catal 2020, 41, 951–962.

(166). Sun C; Li H; Chen L Nanostructured Ceria-Based Materials: Synthesis, Properties, and Applications. Energy Environ. Sci 2012, 5, 8475–8505.

(167). Nolan M; Watson GW The Surface Dependence of CO Adsorption on Ceria. J. Phys. Chem. B 2006, 110, 16600–16606. [PubMed: 16913795]

(168). Lv Y; Li Y; Shen W Synthesis of Co3O4 Nanotubes and Their Catalytic Applications in CO Oxidation. Catal. Commun 2013, 42, 116–120.

(169). Yao HC; Shelef M Nitric Oxide and Carbon Monoxide Chemisorption on Cobalt-Containing Spinels. J. Phys. Chem 1974, 78, 2490–2496.

(170). Wang YG; Yang XF; Li J Theoretical Studies of CO Oxidation with Lattice Oxygen on Co3O4 Surfaces. Cuihua Xuebao/Chin. J. Catal 2016, 37, 193–198.

(171). Xie X; Li Y; Liu ZQ; Haruta M; Shen W Low-Temperature Oxidation of CO Catalysed by Co 3 O 4 Nanorods. Nature 2009, 458, 746–749. [PubMed: 19360084]

(172). Xie X; Shen W Morphology Control of Cobalt Oxide Nanocrystals for Promoting Their Catalytic Performance. Nanoscale 2009, 1, 50–60. [PubMed: 20644860]

(173). Sun Y; Lv P; Yang JY; He L; Nie JC; Liu X; Li Y Ultrathin Co3O4 Nanowires with High Catalytic Oxidation of CO. Chem. Commun 2011, 47, 11279–11281.

(174). Tang X; Li J; Hao J Synthesis and Characterization of Spinel Co3O4 Octahedra Enclosed by the {1 1 1} Facets. Mater. Res. Bull 2008, 43, 2912–2918.

(175). Wang J; Qiao Z; Zhang L; Shen J; Li R; Yang G; Nie F Controlled Synthesis of Co3O4 Single-Crystalline Nanofilms Enclosed by (111) Facets and Their Exceptional Activity for the Catalytic Decomposition of Ammonium Perchlorate. CrystEngComm 2014, 16, 8673–8677.

(176). Yu Y; Takei T; Ohashi H; He H; Zhang X; Haruta M Pretreatments of Co3O4 at Moderate Temperature for CO Oxidation at −80 °C. J. Catal 2009, 267, 121–128.

(177). Niu Z; Li Y Removal and Utilization of Capping Agents in Nanocatalysis. Chem. Mater 2014, 26, 72–83.

(178). Hou L; Zhang Q; Jérôme F; Duprez D; Can F; Courtois X; Zhang H; Royer S Ionic Liquid-Mediated α-Fe2O3 Shape-Controlled Nanocrystal-Supported Noble Metals: Highly Active Materials for CO Oxidation. ChemCatChem 2013, 5, 1978–1988.

(179). Chen S; Takata T; Domen K Particulate Photocatalysts for Overall Water Splitting. Nat. Rev. Mater 2017, 2, 1–17.

(180). Kudo A; Miseki Y Heterogeneous Photocatalyst Materials for Water Splitting. Chem. Soc. Rev 2009, 38, 253–278. [PubMed: 19088977]

(181). Roger I; Shipman MA; Symes MD Earth-Abundant Catalysts for Electrochemical and Photoelectrochemical Water Splitting. Nat. Rev. Chem 2017, 1, 0003.

(182). Wang S; Liu G; Wang L Crystal Facet Engineering of Photoelectrodes for Photoelectrochemical Water Splitting. Chem. Rev 2019, 119, 5192–5247. [PubMed: 30875200]

(183). Shiva Kumar S; Himabindu V Hydrogen Production by PEM Water Electrolysis – A Review. Mater. Sci. Energy Technol 2019, 2, 442–454.

(184). Surendranath Y; Dincă M; Nocera DG Electrolyte-Dependent Electrosynthesis and Activity of Cobalt-Based Water Oxidation Catalysts. J. Am. Chem. Soc 2009, 131, 2615–2620. [PubMed: 19183057]

(185). Wang J; van Ree T; Wu Y; Zhang P; Gao L Metal Oxide Semiconductors for Solar Water Splitting, Metal Oxides in Energy Technologies, 1st ed.; The Metal Oxides Book Series; Elsevier: Cambridge, MA, USA, 2018; 205–249, DOI: 10.1016/b978-0-12-811167-3.00008-0.

(186). FUJISHIMA A; HONDA K Electrochemical Photolysis of Water at a Semiconductor Electrode. Nature 1972, 238, 37–38. [PubMed: 12635268]

(187). Walter MG; Warren EL; McKone JR; Boettcher SW; Mi Q; Santori EA; Lewis NS Solar Water Splitting Cells. Chem. Rev 2010, 110, 6446–6473. [PubMed: 21062097]

(188). Yu J; Qi L; Jaroniec M Hydrogen Production by Photocatalytic Water Splitting over Pt/TiO2 Nanosheets with Exposed (001) Facets. J. Phys. Chem. C 2010, 114, 13118–13125.

(189). Bajdich M; García-Mota M; Vojvodic A; Nørskov JK; Bell AT Theoretical Investigation of the Activity of Cobalt Oxides for the Electrochemical Oxidation of Water. J. Am. Chem. Soc 2013, 135, 13521–13530. [PubMed: 23944254]

(190). Gu X-K; Camayang JCA; Samira S; Nikolla E Oxygen Evolution Electrocatalysis Using Mixed Metal Oxides Under Acidic Conditions: Challenges and Opportunities. J. Catal 2020, 388, 130–140.

(191). Song F; Bai L; Moysiadou A; Lee S; Hu C; Liardet L; Hu X Transition Metal Oxides as Electrocatalysts for the Oxygen Evolution Reaction in Alkaline Solutions: An Application-Inspired Renaissance. J. Am. Chem. Soc 2018, 140, 7748–7759. [PubMed: 29788720]

(192). Samira S; Gu XK; Nikolla E Design Strategies for Efficient Nonstoichiometric Mixed Metal Oxide Electrocatalysts: Correlating Measurable Oxide Properties to Electrocatalytic Performance. ACS Catal. 2019, 9, 10575–10586.

(193). Huang ZF; Wang J; Peng Y; Jung CY; Fisher A; Wang X Design of Efficient Bifunctional Oxygen Reduction/Evolution Electrocatalyst: Recent Advances and Perspectives. Adv. Energy Mater 2017, 7, 1700544.

(194). Bao J; Zhang X; Fan B; Zhang J; Zhou M; Yang W; Hu X; Wang H; Pan B; Xie Y Ultrathin Spinel-Structured Nanosheets Rich in Oxygen Deficiencies for Enhanced Electrocatalytic Water Oxidation. Angew. Chem., Int. Ed 2015, 54, 7399–7404.

(195). Wang Y; Zhou T; Jiang K; Da P; Peng Z; Tang J; Kong B; Cai W-B; Yang Z; Zheng G Reduced Mesoporous Co3O4 Nanowires as Efficient Water Oxidation Electrocatalysts and Supercapacitor Electrodes. Adv. Energy Mater 2014, 4, 1400696.

(196). Zhang M; De Respinis M; Frei H Time-Resolved Observations of Water Oxidation Intermediates on a Cobalt Oxide Nanoparticle Catalyst. Nat. Chem 2014, 6, 362–367. [PubMed: 24651205]

(197). Su D; Dou S; Wang G Single Crystalline Co_3O_4 Nanocrystals Exposed with Different Crystal Planes for Li-O_2 Batteries. Sci. Rep 2015, 4, 5767.

(198). Han X; He G; He Y; Zhang J; Zheng X; Li L; Zhong C; Hu W; Deng Y; Ma TY Engineering Catalytic Active Sites on Cobalt Oxide Surface for Enhanced Oxygen Electrocatalysis. Adv. Energy Mater 2018, 8, 1702222.

(199). Song K; Cho E; Kang YM Morphology and Active-Site Engineering for Stable Round-Trip Efficiency Li-O2 Batteries: A Search for the Most Active Catalytic Site in Co3O4. ACS Catal. 2015, 5, 5116–5122.

(200). Xu Y; Zhang F; Sheng T; Ye T; Yi D; Yang Y; Liu S; Wang X; Yao J Clarifying the Controversial Catalytic Active Sites of Co3O4 for the Oxygen Evolution Reaction. J. Mater. Chem. A 2019, 7, 23191–23198.

(201). Wang HY; Hung SF; Chen HYHM; Chan TS; Chen HYHM; Liu B In *Operando* Identification of Geometrical-Site-Dependent Water Oxidation Activity of Spinel Co3O4. J. Am. Chem. Soc 2016, 138, 36–39. [PubMed: 26710084]

(202). Zandi O; Hamann TW Determination of Photoelectrochemical Water Oxidation Intermediates on Haematite Electrode Surfaces Using *Operando* Infrared Spectroscopy. Nat. Chem 2016, 8, 778–783. [PubMed: 27442283]

(203). Vilé G; Bridier B; Wichert J; Pérez-Ramírez J Ceria in Hydrogenation Catalysis: High Selectivity in the Conversion of Alkynes to Olefins. Angew. Chem., Int. Ed 2012, 51, 8620–8623.

(204). Medford AJ; Vojvodic A; Hummelshøj JS; Voss J; Abild-Pedersen F; Studt F; Bligaard T; Nilsson A; Nørskov JK From the Sabatier Principle to a Predictive Theory of Transition-Metal Heterogeneous Catalysis. J. Catal 2015, 328, 36–42.

(205). Degler D; Weimar U; Barsan N Current Understanding of the Fundamental Mechanisms of Doped and Loaded Semiconducting Metal-Oxide-Based Gas Sensing Materials. ACS Sensors 2019, 4, 2228–2249. [PubMed: 31365820]

(206). Dey A Semiconductor Metal Oxide Gas Sensors: A Review. Mater. Sci. Eng., B 2018, 229, 206–217.

(207). Ji H; Zeng W; Li Y Gas Sensing Mechanisms of Metal Oxide Semiconductors: A Focus Review. Nanoscale 2019, 11, 22664–22684. [PubMed: 31755888]

(208). Al-Hashem M; Akbar S; Morris P Role of Oxygen Vacancies in Nanostructured Metal-Oxide Gas Sensors: A Review. Sens. Actuators, B 2019, 301, 126845.

(209). Korotcenkov G; Ivanov M; Blinov I; Stetter JR Kinetics of Indium Oxide-Based Thin Film Gas Sensor Response: The Role of “Redox” and Adsorption/Desorption Processes in Gas Sensing Effects. Thin Solid Films 2007, 515, 3987–3996.

(210). Li Z; Li H; Wu Z; Wang M; Luo J; Torun H; Hu P; Yang C; Grundmann M; Liu X; Fu Y Advances in Designs and Mechanisms of Semiconducting Metal Oxide Nanostructures for High-Precision Gas Sensors Operated at Room Temperature. Mater. Horiz 2019, 6, 470–506.

(211). Kim HJ; Lee JH Highly Sensitive and Selective Gas Sensors Using *P*-Type Oxide Semiconductors: Overview. Sens. Actuators, B 2014, 192, 607–627.

(212). Miller DR; Akbar SA; Morris PA Nanoscale Metal Oxide-Based Heterojunctions for Gas Sensing: A Review. Sens. Actuators, B 2014, 204, 250–272.

(213). Hübner M; Simion CE; Tomescu-Stănoiu A; Pokhrel S; Bârsan N; Weimar U Influence of Humidity on CO Sensing with *P*-Type CuO Thick Film Gas Sensors. Sens. Actuators, B 2011, 153, 347–353.

(214). Dey A Semiconductor Metal Oxide Gas Sensors: A Review. Mater. Sci. Eng., B 2018, 229, 206–217.

(215). Farfan-Arribas E; Madix RJ Role of Defects in the Adsorption of Aliphatic Alcohols on the TiO2(110) Surface. J. Phys. Chem. B 2002, 106, 10680–10692.

(216). Xu J; Xue Z; Qin N; Cheng Z; Xiang Q The Crystal Facet-Dependent Gas Sensing Properties of ZnO Nanosheets: Experimental and Computational Study. Sens. Actuators, B 2017, 242, 148–157.

(217). Yang Y; Ma H; Zhuang J; Wang X Morphology-Controlled Synthesis of Hematite Nanocrystals and Their Facet Effects on Gas Sensing Properties. Inorg. Chem 2011, 50, 10143–10151. [PubMed: 21923125]

(218). Wang C; Cai D; Liu B; Li H; Wang D; Liu Y; Wang L; Wang Y; Li Q; Wang T Ethanol-Sensing Performance of Tin Dioxide Octahedral Nanocrystals with Exposed High-Energy {111} and {332} Facets. J. Mater. Chem. A 2014, 2, 10623–10628.

(219). Zhao Q; Shen Q; Yang F; Zhao H; Liu B; Liang Q; Wei A; Yang H; Liu S Direct Growth of ZnO Nanodisk Networks with an Exposed (0 0 0 1) Facet on Au Comb-Shaped Interdigitating Electrodes and the Enhanced Gas-Sensing Property of Polar {0 0 0 1} Surfaces. Sens. Actuators, B 2014, 195, 71–79.

(220). Han XG; He HZ; Kuang Q; Zhou X; Zhang XH; Xu T; Xie ZX; Zheng LS Controlling Morphologies and Tuning the Related Properties of Nano/Microstructured ZnO Crystallites. J. Phys. Chem. C 2009, 113, 584–589.

(221). Kaneti YV; Yue J; Jiang X; Yu A Controllable Synthesis of ZnO Nanoflakes with Exposed (1010) for Enhanced Gas Sensing Performance. J. Phys. Chem. C 2013, 117, 13153–13162.

(222). Zhou Q; Zeng W Shape Control of Co3O4Micro-Structures for High-Performance Gas Sensor. Phys. E 2018, 95, 121–124.

(223). Wang L; Zhang R; Zhou T; Lou Z; Deng J; Zhang T *P*-Type Octahedral Cu2O Particles with Exposed {111} Facets and Superior CO Sensing Properties. Sens. Actuators, B 2017, 239, 211–217.

(224). Li X; Wei W; Wang S; Kuai L; Geng B Single-Crystalline α-Fe2O3 Oblique Nanoparallelepipeds: High-Yield Synthesis, Growth Mechanism and Structure Enhanced Gas-Sensing Properties. Nanoscale 2011, 3, 718–724. [PubMed: 21072436]

(225). Sun L; Han XX; Liu K; Yin S; Chen Q; Kuang Q; Han XX; Xie Z; Wang C Template-Free Construction of Hollow α-Fe2O3 Hexagonal Nanocolumn Particles with an Exposed Special Surface for Advanced Gas Sensing Properties. Nanoscale 2015, 7, 9416–9420. [PubMed: 25959552]

(226). Bargar JR; Towle SN; Brown GE; Parks GA XAFS and Bond-Valence Determination of the Structures and Compositions of Surface Functional Groups and Pb(II) and Co(II) Sorption Products on Single-Crystal α-Al2O3. J. Colloid Interface Sci 1997, 185, 473–492. [PubMed: 9028903]

(227). Brown GE; Henrich VE; Casey WH; Clark DL; Eggleston C; Felmy A; Goodman DW; Grätzel M; Maciel G; McCarthy MI; Nealson KH; Sverjensky DA; Toney MF; Zachara JM Metal Oxide Surfaces and Their Interactions with Aqueous Solutions and Microbial Organisms. Chem. Rev 1999, 99, 77–174. [PubMed: 11848981]

(228). Fendorf S; Eick MJ; Grossl P; Sparks DL Arsenate and Chromate Retention Mechanisms on Goethite. 1. Surface Structure. Environ. Sci. Technol 1997, 31, 315–320.

(229). Kang D; Yu X; Ge M Morphology-Dependent Properties and Adsorption Performance of CeO2 for Fluoride Removal. Chem. Eng. J 2017, 330, 36–43.

(230). Yu XY; Meng QQ; Luo T; Jia Y; Sun B; Li QX; Liu JH; Huang XJ Facet-Dependent Electrochemical Properties of Co 3 O 4 Nanocrystals toward Heavy Metal Ions. Sci. Rep 2013, 3, 1–7.

(231). Mishra AK; Pradhan D Morphology Controlled Solution-Based Synthesis of Cu2O Crystals for the Facets-Dependent Catalytic Reduction of Highly Toxic Aqueous Cr(VI). Cryst. Growth Des 2016, 16, 3688–3698.

(232). Sugimoto T; Wang YS Mechanism of the Shape and Structure Control of Monodispersed Fe_2O_3 Particles by Sulfate Ions. J. Colloid Interface Sci 1998, 207, 137–149. [PubMed: 9778401]

(233). Lounsbury AW; Wang R; Plata DL; Billmyer N; Muhich C; Kanie K; Sugimoto T; Peak D; Zimmerman JB Preferential Adsorption of Selenium Oxyanions onto {1 1 0} and {0 1 2} Nano-Hematite Facets. J. Colloid Interface Sci 2019, 537, 465–474. [PubMed: 30469115]

(234). Mei H; Liu Y; Tan X; Feng J; Ai Y; Fang M. U(VI) Adsorption on Hematite Nanocrystals: Insights into the Reactivity of {001} and {012} Facets. J. Hazard. Mater 2020, 399, 123028. [PubMed: 32521314]

(235). Lv J; Miao Y; Huang Z; Han R; Zhang S Facet-Mediated Adsorption and Molecular Fractionation of Humic Substances on Hematite Surfaces. Environ. Sci. Technol 2018, 52, 11660–11669. [PubMed: 30222318]

(236). Zhai H; Wang L Single-Molecule Determination of the Phase-A Nd Facet-Dependent Adsorption of Alginate on Iron Oxides. Environ. Sci.: Nano 2020, 7, 954–962.

(237). Shen Z; Zhang Z; Li T; Yao Q; Zhang T; Chen W Facet-Dependent Adsorption and Fractionation of Natural Organic Matter on Crystalline Metal Oxide Nanoparticles. Environ. Sci. Technol 2020, 54, 8622–8631. [PubMed: 32539365]

(238). Li T; Zhong W; Jing C; Li X; ZHANG T; Jiang C; Chen W Enhanced Hydrolysis of P-Nitrophenyl Phosphate by Iron (Hydr)Oxide Nanoparticles: Roles of Exposed Facets. Environ. Sci. Technol 2020, 54, 8658. [PubMed: 32545958]

(239). Zhang H; Wang W; Zhao H; Zhao L; Gan LY; Guo LH Facet-Mediated Interaction between Humic Acid and TiO2 Nanoparticles: Implications for Aggregation and Stability Kinetics in Aquatic Environments. Environ. Sci.: Nano 2019, 6, 1754–1764.

(240). Song J; Yan L; Duan J; Jing C TiO2 Crystal Facet-Dependent Antimony Adsorption and Photocatalytic Oxidation. J. Colloid Interface Sci 2017, 496, 522–530. [PubMed: 28259018]

(241). Yan L; Du J; Jing C How TiO2 Facets Determine Arsenic Adsorption and Photooxidation: Spectroscopic and DFT Studies. Catal. Sci. Technol 2016, 6, 2419–2426.

(242). Chen K; Chen C; Ren X; Alsaedi A; Hayat T Interaction Mechanism between Different Facet TiO2 and U(VI): Experimental and Density-Functional Theory Investigation. Chem. Eng. J 2019, 359, 944–954.

(243). Barrón V; Torrent J Surface Hydroxyl Configuration of Various Crystal Faces of Hematite and Goethite. J. Colloid Interface Sci 1996, 177, 407–410.

(244). Hiemstra T; Venema P; Riemsdijk WHV Intrinsic Proton Affinity of Reactive Surface Groups of Metal (Hydr)Oxides: The Bond Valence Principle. J. Colloid Interface Sci 1996, 184, 680–692. [PubMed: 8978574]

(245). Venema P; Hiemstra T; Weidler PG; Van Riemsdijk WH Intrinsic Proton Affinity of Reactive Surface Groups of Metal (Hydr)Oxides: Application to Iron (Hydr)Oxides. J. Colloid Interface Sci 1998, 198, 282–295.

(246). Casey WH; Swaddle TW Why Small? The Use of Small Inorganic Clusters to Understand Mineral Surface and Dissolution Reactions in Geochemistry. Rev. Geophys 2003, 41, 1008.

(247). Catalano JG; Zhang Z; Fenter P; Bedzyk MJ Inner-Sphere Adsorption Geometry of Se(IV) at the Hematite (100)-Water Interface. J. Colloid Interface Sci 2006, 297, 665–671. [PubMed: 16386265]

(248). Pincus LN; Rudel HE; Petrović PV; Gupta S; Westerhoff P; Muhich CL; Zimmerman JB Exploring the Mechanisms of Selectivity for Environmentally Significant Oxo-Anion Removal during Water Treatment: A Review of Common Competing Oxo-Anions and Tools for Quantifying Selective Adsorption. Environ. Sci. Technol 2020, 54, 9769–9790. [PubMed: 32515947]

(249). Wang WW; Yu WZ; Du PP; Xu H; Jin Z; Si R; Ma C; Shi S; Jia CJ; Yan CH Crystal Plane Effect of Ceria on Supported Copper Oxide Cluster Catalyst for CO Oxidation: Importance of Metal-Support Interaction. ACS Catal. 2017, 7, 1313–1329.

(250). Hu Z; Liu X; Meng D; Guo YY; Guo YY; Lu G Effect of Ceria Crystal Plane on the Physicochemical and Catalytic Properties of Pd/Ceria for CO and Propane Oxidation. ACS Catal. 2016, 6, 2265–2279.

(251). Han J; Meeprasert J; Maitarad P; Nammuangruk S; Shi L; Zhang D Investigation of the Facet-Dependent Catalytic Performance of Fe2O3/CeO2 for the Selective Catalytic Reduction of NO with NH3. J. Phys. Chem. C 2016, 120, 1523–1533.

(252). Liu J; Meeprasert J; Namuangruk S; Zha K; Li H; Huang L; Maitarad P; Shi L; Zhang D Facet-Activity Relationship of TiO2 in Fe2O3/TiO2 Nanocatalysts for Selective Catalytic Reduction of NO with NH3: *in Situ* DRIFTs and DFT Studies. J. Phys. Chem. C 2017, 121, 4970–4979.

(253). Yao X; Kong T; Yu S; Li L; Yang F; Dong L Influence of Different Supports on the Physicochemical Properties and Denitration Performance of the Supported Mn-Based Catalysts for NH 3 -SCR at Low Temperature. Appl Surf. Sci 2017, 402, 208–217.

(254). D'Arienzo M; Carbajo J; Bahamonde A; Crippa M; Polizzi S; Scotti R; Wahba L; Morazzoni F Photogenerated Defects in Shape-Controlled TiO 2 Anatase Nanocrystals: A Probe to Evaluate the Role of Crystal Facets in Photocatalytic Processes. J. Am. Chem. Soc 2011, 133, 17652–17661. [PubMed: 21970524]

(255). Yu J; Low J; Xiao W; Zhou P; Jaroniec M Enhanced Photocatalytic CO2-Reduction Activity of Anatase TiO2 by Coexposed {001} and {101} Facets. J. Am. Chem. Soc 2014, 136, 8839–8842. [PubMed: 24918628]

(256). Roy N; Sohn Y; Pradhan D Synergy of Low-Energy {101} and High-Energy {001} TiO2 Crystal Facets for Enhanced Photocatalysis. ACS Nano 2013, 7, 2532–2540. [PubMed: 23448713]

(257). Sun S; Gao P; Yang Y; Yang P; Chen Y; Wang Y N-Doped TiO2 Nanobelts with Coexposed (001) and (101) Facets and Their Highly Efficient Visible-Light-Driven Photocatalytic Hydrogen Production. ACS Appl. Mater. Interfaces 2016, 8, 18126–18131. [PubMed: 27356016]

(258). Collins G; Davitt F; O'Dwyer C; Holmes JD Comparing Thermal and Chemical Removal of Nanoparticle Stabilizing Ligands: Effect on Catalytic Activity and Stability. ACS Appl. Nano Mater 2018, 1, 7129–7138.

(259). Zhang Y; Chen Y; Westerhoff P; Hristovski K; Crittenden JC Stability of Commercial Metal Oxide Nanoparticles in Water. Water Res. 2008, 42, 2204–2212. [PubMed: 18164742]

(260). Tso C; Zhung C; Shih Y; Tseng Y-M; Wu S; Doong R Stability of Metal Oxide Nanoparticles in Aqueous Solutions. Water Sci. Technol 2010, 61, 127–133. [PubMed: 20057098]

(261). Hotze EM; Phenrat T; Lowry GV Nanoparticle Aggregation: Challenges to Understanding Transport and Reactivity in the Environment. J. Environ. Qual 2010, 39, 1909–1924. [PubMed: 21284288]

(262). Wang XG; Weiss W; Shaikhutdinov SK; Ritter M; Petersen M; Wagner F; Schlögl R; Scheffler M The Hematite (α-Fe2O3) (0001) Surface: Evidence for Domains of Distinct Chemistry. Phys. Rev. Lett 1998, 81, 1038–1041.

(263). Back S; Tran K; Ulissi ZW Toward a Design of Active Oxygen Evolution Catalysts: Insights from Automated Density Functional Theory Calculations and Machine Learning. ACS Catal. 2019, 9, 7651–7659.

(264). Núñez M; Lansford JL; Vlachos DG Optimization of the Facet Structure of Transition-Metal Catalysts Applied to the Oxygen Reduction Reaction. Nat. Chem 2019, 11, 449–456. [PubMed: 30962608]

(265). Payne MC; Teter MP; Allan DC; Arias TA; Joannopoulos JD Iterative Minimization Techniques for *Ab Initio* Total-Energy Calculations: Molecular Dynamics and Conjugate Gradients. Rev. Mod. Phys 1992, 64, 1045–1097.

(266). Tomasi J; Mennucci B; Cammi R Quantum Mechanical Continuum Solvation Models. Chem. Rev 2005, 105, 2999–3094. [PubMed: 16092826]

(267). Perdew JP; Burke K; Ernzerhof M Generalized Gradient Approximation Made Simple. Phys. Rev. Lett 1996, 77, 3865–3868. [PubMed: 10062328]

(268). Heyd J; Scuseria GE; Ernzerhof M Hybrid Functionals Based on a Screened Coulomb Potential. J. Chem. Phys 2003, 118, 8207–8215.

(269). Hubbard J; Flowers BH Electron Correlations in Narrow Energy Bands. Proc. R. Soc. London, Ser. A 1963, 276, 238–257.

(270). Li T; Shen Z; Shu Y; Li X; Jiang C; Chen W Facet-Dependent Evolution of Surface Defects in Anatase TiO2 by Thermal Treatment: Implications for Environmental Applications of Photocatalysis. Environ. Sci.: Nano 2019, 6, 1740–1753.

(271). Iwasawa Y, Asakura K, Tada M, Eds. XAFS Techniques for Catalysts, Nanomaterials, and Surfaces, 1st ed.; Springer: Cham, Switzerland, 2017; DOI: 10.1007/978-3-319-43866-5.

(272). Catalano JG; Trainor TP; Eng PJ; Waychunas GA; Brown GE CTR Diffraction and Grazing-Incidence EXAFS Study of U(VI) Adsorption onto α-Al2O3 and α-Fe2O3 (1102) Surfaces. Geochim. Cosmochim. Acta 2005, 69, 3555–3572.

(273). Lykaki M; Pachatouridou E; Carabineiro SAC; Iliopoulou E; Andriopoulou C; Kallithrakas-Kontos N; Boghosian S; Konsolakis M Ceria Nanoparticles Shape Effects on the Structural Defects and Surface Chemistry: Implications in CO Oxidation by Cu/CeO2 Catalysts. Appl. Catal., B 2018, 230, 18–28.

(274). Sartoretti E; Novara C; Fontana M; Giorgis F; Piumetti M; Bensaid S; Russo N; Fino D New Insights on the Defect Sites Evolution during CO Oxidation over Doped Ceria Nanocatalysts Probed by *in Situ* Raman Spectroscopy. Appl. Catal., A 2020, 596, 117517.

(275). Peng YK; Tsang SCE Facet-Dependent Photocatalysis of Nanosize Semiconductive Metal Oxides and Progress of Their Characterization. Nano Today 2018, 18, 15–34.

(276). Chen S; Cao T; Gao Y; Li D; Xiong F; Huang W Probing Surface Structures of CeO2, TiO2, and Cu2O Nanocrystals with CO and CO2 Chemisorption. J. Phys. Chem. C 2016, 120, 21472–21485.

(277). Yin Z-W; Betzler SB; Sheng T; Zhang Q; Peng X; Shangguan J; Bustillo KC; Li J-T; Sun S-G; Zheng H Visualization of Facet-Dependent Pseudo-Photocatalytic Behavior of TiO2 Nanorods for Water Splitting Using *in Situ* Liquid Cell TEM. Nano Energy 2019, 62, 507–512.

(278). Crozier PA; Wang R; Sharma R *In Situ* Environmental TEM Studies of Dynamic Changes in Cerium-Based Oxides Nanoparticles during Redox Processes. Ultramicroscopy 2008, 108, 14321440.

(279). Wu J; Shan H; Chen W; Gu X; Tao P; Song C; Shang W; Deng T *In Situ* Environmental TEM in Imaging Gas and Liquid Phase Chemical Reactions for Materials Research. Adv. Mater 2016, 28, 9686–9712. [PubMed: 27628711]

(280). Liu J; Fung V; Wang Y; Du K; Zhang S; Nguyen L; Tang Y; Fan J; Jiang D. en; Tao FF. Promotion of Catalytic Selectivity on Transition Metal Oxide through Restructuring Surface Lattice. Appl. Catal., B 2018, 237, 957–969.

(281). Walker JM; Akbar SA; Morris PA Synergistic Effects in Gas Sensing Semiconducting Oxide Nano-Heterostructures: A Review. Sens. Actuators, B 2019, 286, 624–640.

(282). Jia QQ; Ji HM; Wang DH; Bai X; Sun XH; Jin ZG Exposed Facets Induced Enhanced Acetone Selective Sensing Property of Nanostructured Tungsten Oxide. J. Mater. Chem. A 2014, 2, 13602–13611.

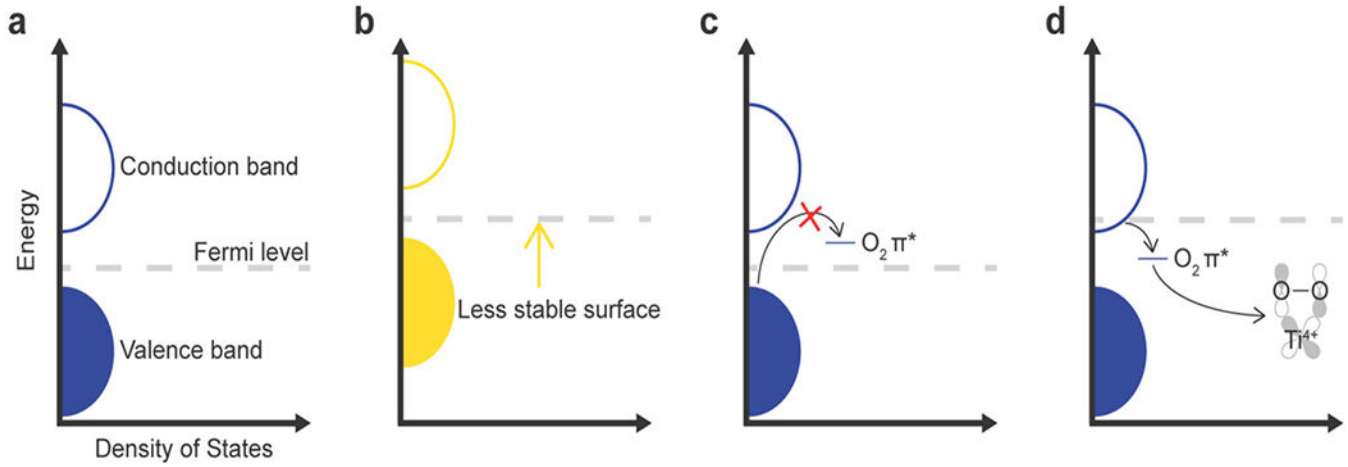

Figure 1.

(a) Schematic representation of a density of states plot of a semiconducting surface with the number of orbitals or bands (*i.e.*, density of states) at a given energy level, and which states are occupied or empty, as shown by the Fermi level; (b) high-energy semiconducting surface; (c) interaction between O_2 and the metal oxide surface where bonding does not occur; (d) interactions between O_2 and a metal oxide surface where bonding would occur.

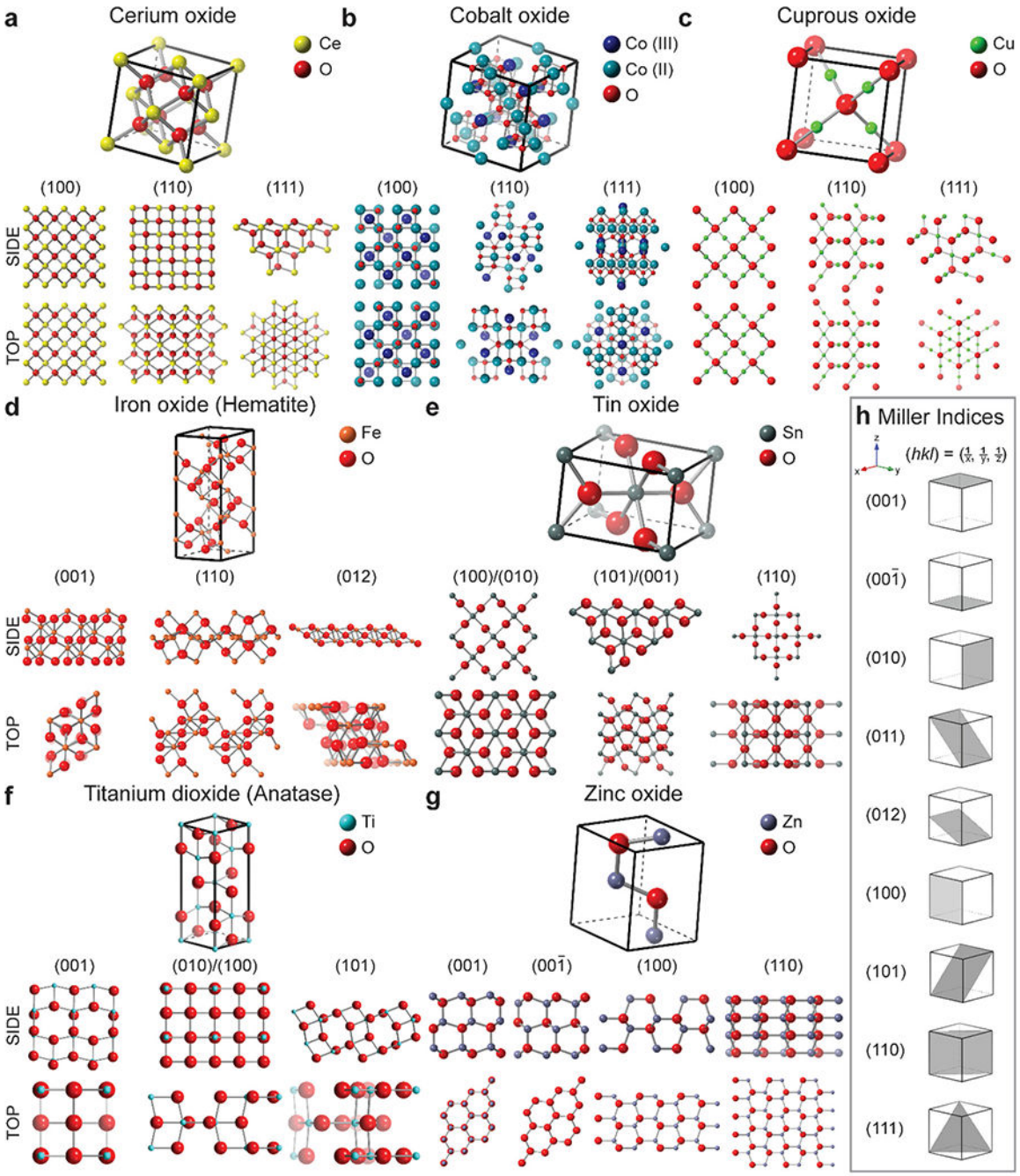

Figure 2.

(Top) Atomic crystal structure with unit cell and respective facet surface structures (middle, side views; bottom, top views) of nanoscale metal oxides: (a) cerium oxide, (b) cobalt oxide, (c) cuprous oxide, (d) iron oxide (hematite), (e) tin oxide, (f) titanium dioxide (anatase), and (g) zinc oxide. (h) Common low-index crystal planes or facets identified by Miller indices. All structures were generated using CrystalMaker X software. Crystallographic data for each structure, in CIF format, is located in the Supporting Information.

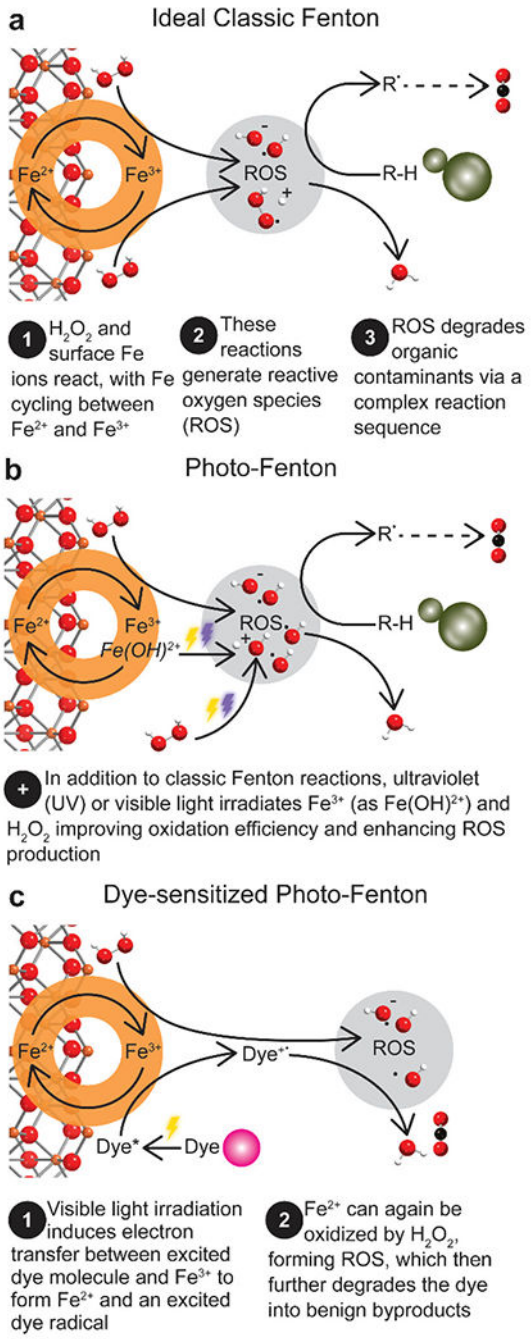

Figure 3.

Fenton and Fenton-like reactions illustrated over the hematite (001) facet (side view): (a) classic Fenton reaction; (b) Fenton-like photo-Fenton reaction; (c) Fenton-like dye-sensitized photo-Fenton reaction.

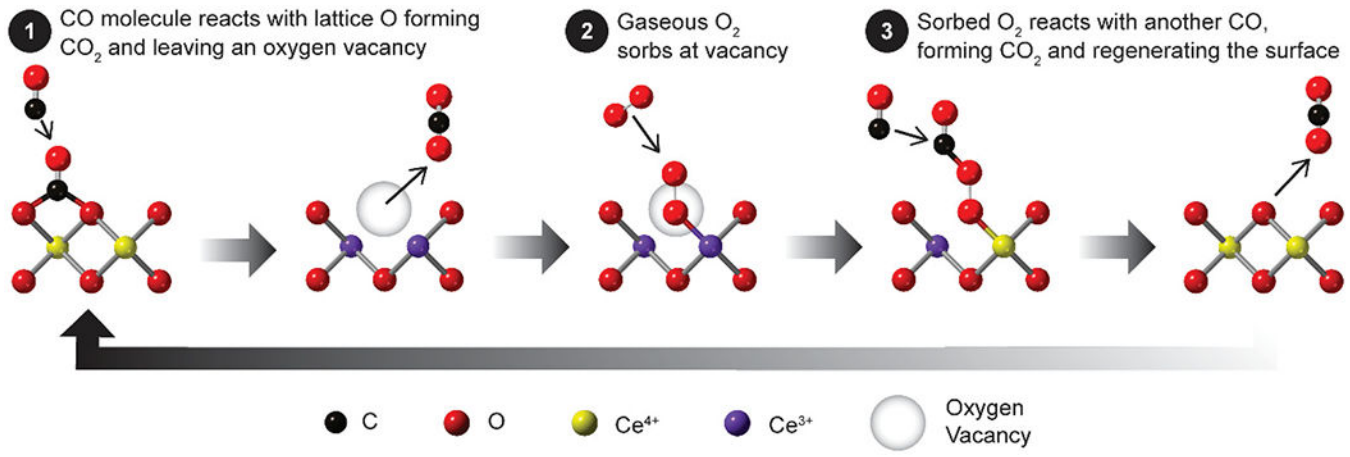

Figure 4.

CO oxidation *via* the Mars–van Krevelen mechanism, represented here on ceria's (100) facet (side view).

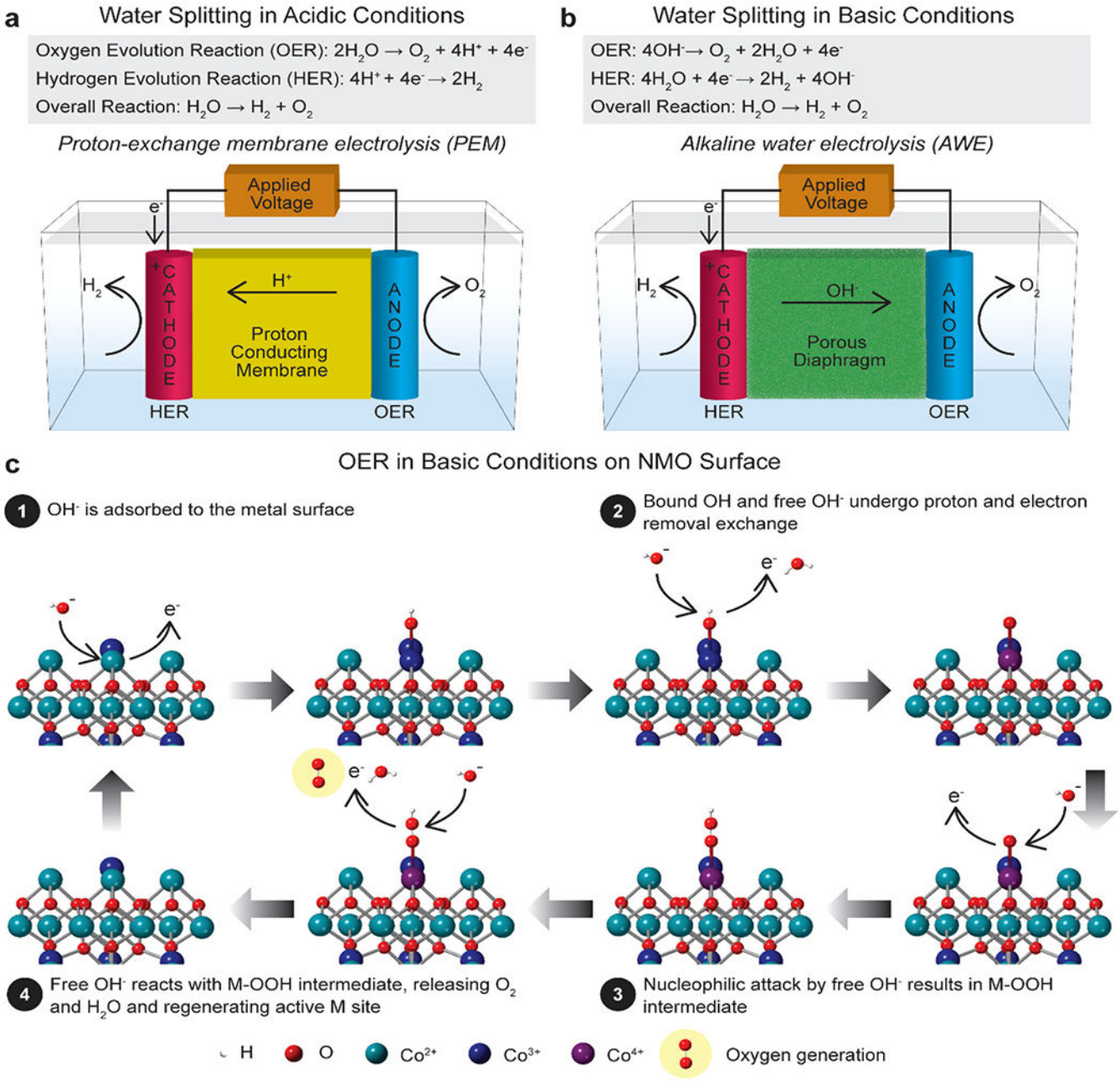

Figure 5.

Water splitting in (a) acidic conditions and (b) basic conditions illustrated with schematics of proton-exchange electrolysis (PEM) and alkaline water electrolysis (AWE), respectively. Oxygen evolution reaction (OER) in (c) basic conditions illustrated over Co_3O_4 (111) facet (side view). OER in acidic conditions is thermodynamically equivalent to basic conditions and follows the same general sorption sequence with substitution of H_2O and H^+ where appropriate.

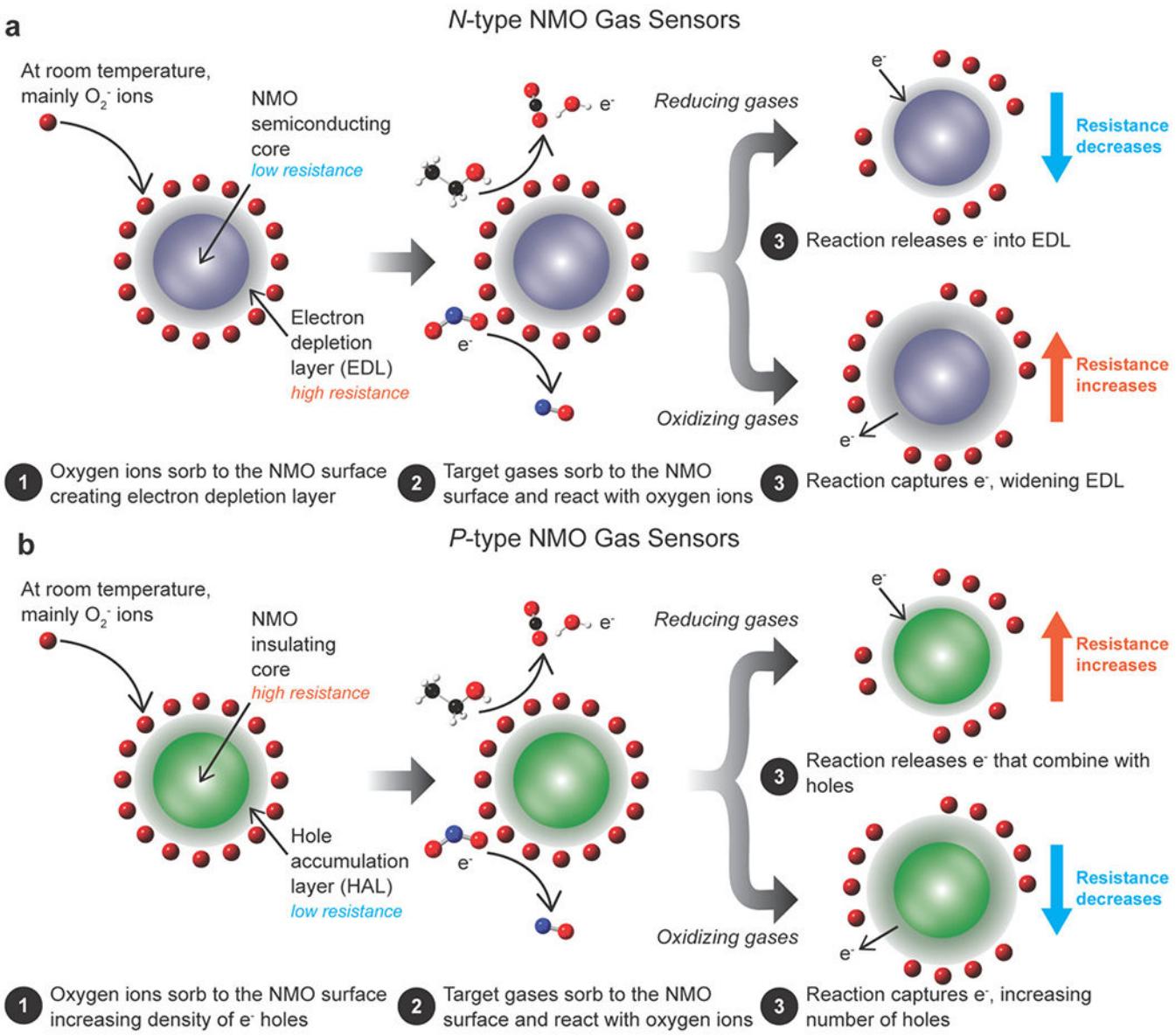

Figure 6.

Characteristics and gas sensing mechanisms of (a) n-type and (b) p-type gas sensors for both oxidizing and reducing gases.

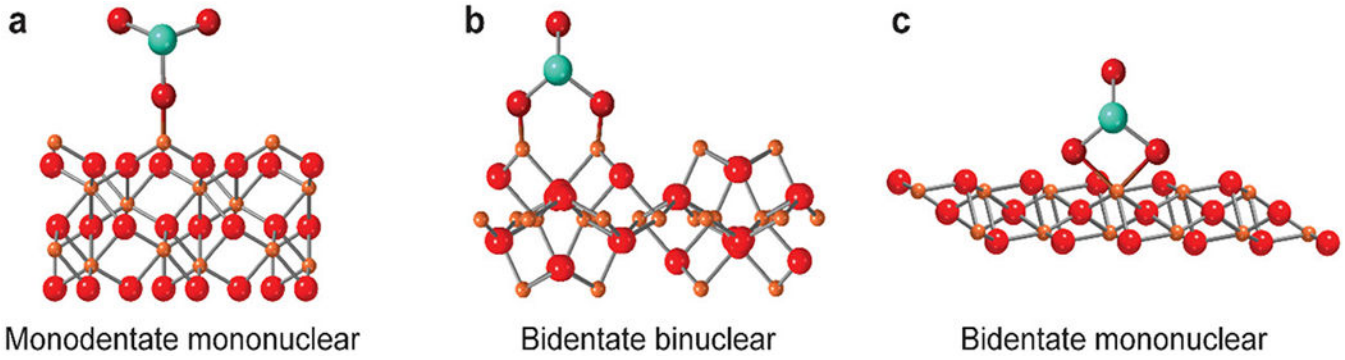

Figure 7.

Common types of direct sorption of contaminants on NMOs: (a) monodentate mononuclear, (b) bidentate binuclear, and (c) bidentate mononuclear, shown on iron oxide hematite (001), (110), and (012) facets, respectively (side views).

Table 1.

Facet Reactivity of NMOs in Catalytic Applications

application	NMO	target molecule	facet 1 <	facet 2 <	facet 3	ref	notes
Fenton and Fenton-like catalysis	CeO_2	*p*-nitrophenol	{111}	{100}	{110}	103	ozone as reducing agent
		orange II	{111}	{100}	{110}	31	
		methylene blue	{111}	{110}	{100}	39	
		hydroxyl radical production from H_2O_2	{111}	{100}	{110}	104	same order as V_o density
	Co_3O_4	H_2O_2 degradation	{100}	{110}	{112}	105	
		3,3′,5,5′-tetramethylbenzidine	{100}	{110}	{112}	106	
	Cu_2O	methyl orange		{100}	{111}	107	
		methyl orange		{100}	{110}	99	no degradation of methylene blue
		methyl orange	{100}	{111}	{110}	108	
		methyl orange	{110}	{100}	{111}	109	
		methyl orange		{100}	{111}	110	no degradation of methylene blue or methyl violet
		methyl orange		{100}	{111}	111	
		methyl orange		{100}	{111}	112	
	α-Fe_2O_3	rhodamine B	{001}	{012}	{110}	113	
		rhodamine B	{001} + {100}	{012}		114	
		rhodamine B	{012}	{104}		115	
		rhodamine B	{012}	{001}		72	
		rhodamine B	{001}	{110}		116	confined ferrous ions
		methylene blue	{001}	{101}		117	
		methylene blue	{001}	{104}	{113}	118	
		Alachor	{012}	{001}		119	
		methyl orange	{012}	{001} + {110}	{101} + {001}	120	
	ZnO	methyl orange	O-terminated {001}	Zn-terminated {001}	{100}	121	
CO and organic molecule oxidation	CeO_2	CO	{111}	{100}	{110}	41	
		oxygen storage capacity	{111}	{110}	{100}	122	

application	NMO	target molecule	facet 1 <	facet 2 <	facet 3	ref	notes
		CO	{111}	{110} + {100}		12	
		CO	{111}	{110} + {100}		123	
		propane oxidation	{110} + {100}	{100}		43	
	Co_3O_4	CO	{100}	{110}	{111}	124	
		CO	{001}	{011}		125	
		methane combustion	{001}	{011}	{112}	7	
		methane combustion	{100}	{111}		126	
		ethylene oxidation	{112}	{110}		127	
		ammonium perchlorate decomposition	{100}	{111}	{110}	128	
	Cu_2O	CO	{100}	{111}	{110}	129	
		CO	{100}	{110}	{111}	130	
		CO	{100}	{111}		131	
		propylene oxidation	{111} planes selective for formation of acrolein (Cu(I) active site) {100} planes selective for CO_2 formation (doubly coordinated O active site) {110} planes selective for propylene oxide (triply coordinated O active site)			132	
	α-Fe_2O_3	CO	{001}	{012}	{110}	133	
		CO	{001}	{113}	{012}	134	
		CO	{001}	{012}	{110}	135	
	SnO_2	CO	{110}	{101}	{111}	85	
water splitting	Co_3O_4	H_2O (OER)	{100}	{110} = {112}		136	photocatalytic OER with $[Ru(bpy)_3]^{2+}$ as photosensitizer and $Na_2S_2O_8$ as oxidant
		H_2O (OER)	{100}	{110} = {112}		136	electrocatalytic
		H_2O (OER)	{100}	{111}		56	electrocatalytic
		H_2O (OER)	{100} & {111}	{110}		50	electrocatalytic
		O_2 (HER)	{100}	{111}	{110}	50	electrocatalytic
		H_2O (OER)/(HER)	{001}	{110}	{111}	137	electrocatalytic
	α-Fe_2O_3	H_2O (OER)	{001}	{012}[a]		138	PEC cell
		H_2O (OER)	{110}	{104}	{012}	139	electrocatalytic
		H_2O (OER)	{012}	{113}	{001}	140	electrocatalytic
hydrogenation	CeO_2	propene and propyne hydrogenation	{110}	{100}	{111}	141	low selectivity of product

ACS Nano. Author manuscript; available in PMC 2022 May 25.

application	NMO	target molecule	facet 1 <	facet 2 <	facet 3	ref	notes
		acetylene hydrogenation		{110} + {100}	{111}	142	low selectivity to ethylene
		propyne hydrogenation		{110} + {100}	{111}	143	low selectivity to ethylene
	Co_3O_4	carbonyl sulfide hydrogenation	{111} + {100}	{110} + {001}		144	catalysts sulfided before catalytic evaluation
organocatalysis	Cu_2O	synthesis of 3,5-disubstituted isoxazoles	{100}	{111}	{110}	145	
		synthesis of 1,2,3-triazoles	{100}	{111}	{110}	146	
		N-arylation reaction of iodobenzene with imidazole		{100}	{111}	147	catalytic activity improved by selective etching of {100} surface

[a]Correspondingly high rates of charge transfer and recombination.

Table 2.

Reactive Facets for Gas Sensing Applications

semiconductor type	NMO	target molecule(s)	facet 1 <	facet 2 <	facet 3	facet 4	ref
n-type	α-Fe_2O_3	acetone, methanol	{001}	{012}	{113}		134
		acetic acid, ammonia, methanol, acetone, ethanol, formaldehyde	{001}	{012}			217
	SnO_2	ethanol	{111}	{332}			218
		ethanol, acetone	{110}	{101}	{111}	{221}	85
		ethanol	{110}	{221}			86
	ZnO	ammonia, triethylamine, ethanol	{010}	{001}			219
		ethanol	{100}	{001}			216
		ethanol	{101}	{100}	{001}		220
		ethanol	{100}	{001}			221
p-type	Co_3O_4	methanol, ammonia, ethanol, acetone	{100}	{111}			222
	Cu_2O	CO	{100}	{111}			223

ACS Nano. Author manuscript; available in PMC 2022 May 25.

Table 3.

Facet-Dependent Sorption Capacity of Metal Oxides in the Removal of Aqueous Contaminants

NMO	target molecule(s)	facet 1 <	facet 2 <	facet 3	ref	notes
CeO_2	fluoride	{100}	{111}	{111}	229	pH-dependent with max adsorption at pH 3
Co_3O_4	Pb^{2+}	{001}	{111}		230	pH 5
Cu_2O	Cr^{6+} sorption and oxidation		{111}	{100}	231	pH 2, 4, 6
α-Fe_2O_3	Pb^{2+}	{001}	{012}	{110}	76	pH 4
		{001}	{110}	{012}	76	pH 6
	$HCrO_4^-$	{001}	{110}		67	IS 0, 0.01, 0.05, 0.1 M NaCl; pH 2
	SO_4^-	{001}	{110} = {012}		232	pH 1
	$HSeO_3^-$	{012}	{110}		233	IS 0.01 M KCl; pH 3.5
	SeO_4^-	{012}	{110}		233	IS 0.01 M KCl;pH 3.5
	U^{6+}	{001}	{012}		234	pH 5; EXAFS and DFT
	phenylarsonic acid	{001}	{012}		81	pH 7
	humic acid and fulvic acid	{001}	{100}		235	pH 6.5
	alginate	{001}	{110}	{100}	236	AFM and DFT
	humic acid and fulvic acid	{001}	{110}		237	pH 5–9
	4-nitrophenyl phosphate	{001}	{100}		238	pH 5–9
TiO_2 (anatase)	Humic acid and fulvic acid	{001}	{101}		237	pH 5–9
	humic acid	{001}	{101}		239	pH 5.4
	Sb^{3+}	{101}	{100}	{001}	240	pH 7
	As^{3+} sorption and oxidation	{101}	{001}		241	pH 7
	As^{5+}	{101}	{001}		242	pH 7
	U^{6+} sorption and oxidation	{101}	{100}	{001}	242	pH 5